Wwc2 is a novel mitotic/meiotic cell-cycle regulator and cell fate related gene, during preimplantation mouse embryo development and oogenesis.

Giorgio Virnicchi[1*], Pablo Bora[1], Lenka Gahurová[1], Andrej Šušor[2] and Alexander W. Bruce[1*]

[1] Laboratory of Early Mammalian Developmental Biology (LEMDB),
Department of Molecular Biology & Genetics,
Faculty of Science,
University of South Bohemia,
Branišovská 31,
370 05 České Budějovice (Budweis),
CZECH REPUBLIC.

[2] Laboratory of Biochemistry and Molecular Biology of Germ Cells,
Institute of Animal Physiology and Genetics,
Czech Academy of Sciences, Rumburská 89,
277 21 Liběchov,
CZECH REPUBLIC.

[*]correspondence; A.W.B. awbruce@prf.jcu.cz & G.V. giorgio.virnicchi@gmail.com
Tel: +420387772291
Fax: +42038777226 (not confidential)

Keywords: Meiosis, mitosis, chromosome segregation, cytokinesis, cell division, cell fate, preimplantation mouse embryo, blastocyst, oocyte.

ABSTRACT

Derivation of late stage mouse blastocysts (E4.5) marks the end of the preimplantation period, whereby the earliest developmental events are manifest in regulated cell cleavage divisions and formation of three distinct cell lineages. Here we report targeted dysregulated expression of the *Wwc2* gene, an ill characterised paralog of the upstream Hippo-signalling activator *Kibra/Wwc1*, is specifically associated with cell autonomous deficits in embryo cell number and gross division abnormalities/phenotypes; typified by imbalanced daughter cell chromatin segregation. Clonal dysregulation additionally implicates *Wwc2* in maintaining the pluripotent epiblast lineage by the late blastocyst stage. The uncovered early mitotic regulatory role is conserved during mouse oocyte meiotic maturation, whereby *Wwc2* dysregulation blocks progress to the fertilisation competent stage of meiosis II metaphase arrest, with attendant spindle defects and failed Aurora kinase A (AURKA) phosphorylation/activation. All identified *Wwc2* specific cell division phenotypes are fully revertible by expression of recombinant HA-epitope tagged WWC2, that localises to cytokinesis derived mid-body structures and restores activated p-AURKA levels, in embryos and oocytes, respectively. Thus, we have identified *Wwc2* as a novel regulator of both meiotic and early mitotic cell divisions, and subsequently mouse blastocyst cell fate.

INTRODUCTION

Mouse embryo development begins with the fertilisation of ovulated secondary oocytes, appropriately arrested in the metaphase of the second meiotic division (MII-arrested), resulting in the diploid and developmental competent zygote ([1]). Ovulated secondary MII oocytes arise from subpopulations of primary oocytes, that have been arrested in the dictyate stage of prophase of meiosis I (MI) since prenatal development, stimulated by maternal reproductive hormones to re-enter and complete meiosis I (reviewed [2]). In addition to ensuring both the necessary growth required to support later embryonic development and expression of gene products required to execute meiosis, meiotic maturation ensures replicated chromosomal bivalents are appropriately resolved and faithfully segregated between the first polar body and a developmentally competent secondary MII oocyte (endowed with the capacity to subsequently faithfully segregate sister chromatids between the second polar body and resulting zygote, post-fertilisation). Failure to precisely segregate chromosomes, resulting in egg and/or zygotic aneuploidy, has severe and usually terminal consequences for embryonic development, with aneuploidy attributable to the human female germline recorded as the leading single cause of spontaneously aborted pregnancy [3, 4]. An extensive literature covering the varied and integrated molecular mechanisms that underpin the germane segregation of homologous chromosomes in MI exists; ranging across meiotic cell-cycle resumption, germinal vesicle (GV/nuclear envelope) breakdown, meiotic spindle assembly, spindle microtubule-kinetochore attachment, chromosomal congression, functioning of the spindle assembly checkpoint (SAC), regulation of the anaphase promoting complex/cyclosome (APC/C) and regulation of cytokinesis/polar body generation (see comprehensive reviews [2, 5, 6, 7, 8]). In keeping with all mammals, and unlike most mitotic somatic cells, meiotic spindle formation in primary mouse oocytes occurs in the absence of centrioles/centrosomes. Spindle assembly is initiated in the vicinity of condensing chromosomes from coalescing microtubule organising centres (MTOCs) and is further stabilised by chromosome derived RAN-GTP gradients that respectively promote and inhibit microtubule polymerisation and destabilisation [5, 6, 8, 9, 10]. Unlike other mammalian developmental systems, the transition from MTOC initiated spindle formation to centrosomal control in mice only occurs by the mid-blastocysts stage, when centrosomes appear *de novo* ([11]); contrasting with other mammals (*e.g.* humans) were fertilising sperm provide a founder centrosome that ensures the first mitotic spindle is assembled centrosomally [12, 13]. Thus, formation and functioning of the first meiotic, and somewhat uniquely, early mitotic spindles in mice are subject to non-centrosomal based regulation. Amongst known key regulators of spindle dynamics are the conserved Aurora-kinase family proteins (AURKA, AURKB & AURKC, collectively referred to here as AURKs) that all exhibit germ cell and early embryonic expression; although, AURKC is not expressd in other somatic cells [14]. During meiosis, AURKs impart important regulatory roles in spindle formation/ organisation, MTOC clustering, chromosome condensation and alignment, plus correct microtubule-kinetochore attachment, chromosomal cohesion and cytokinesis in mitosis (reviewed in [15]). Specifically, AURKA protein is essential for MI progression [16] and is continually localised with MTOCs and MI/ MII spindle poles, regulating clustering and initiating microtubule nucleation/dynamics, throughout meiosis [15, 17, 18, 19]; with similar roles in post-fertilisation zygotes [20]. Despite the lack of centrosomes, AURKA functionally cooperates with the key centrosomal protein Polo-like kinase 4 (PLK4), to promote meiotic spindle microtubule nucleation [21] and PLK4 participates in MTOC mediated/non-centrosomal mitotic divisions of cleavage stage mouse embryo blastomeres [22].

Over the 4.5 days post MII oocyte fertilisation, a series of asynchronous cell cleavage divisions generates blastocysts capable of uterine implantation, comprising three distinct cell lineages; an outer-residing, differentiating and apical-basolaterally polarised epithelium called the trophectoderm (TE – a progenitor of placental tissue), differentiating primitive endoderm (PrE – precursors of the yolk sac), represented as a polarised superficial mono-layer of inner-cell mass (ICM) cells in contact with the fluid filled cavity and the pluripotent epiblast (EPI – progenitors of subsequent foetal tissue), found completely encapsulated within the ICM (comprehensively reviewed [23, 24, 25, 26, 27, 28]). Characteristically, the cell-cycle dynamics of mouse (indeed, mammalian) preimplantation development are generally distinct from other metazoan species, being atypically long by comparison (reviewed in [29]); comprising 12-14 hours from the 4-cell (E2.0) stage [30, 31, 32, 33], versus the much more rapid early embryonic divisions observed of oviparous species [34, 35, 36]. Elongated early cell-cycles are necessary to facilitate mechanisms of selective embryonic differentiation (towards supportive extraembryonic tissues) required to sustain viviparous development [37]. Amongst such mechanisms is the differential regulation of Hippo-signalling, (originally identified in *Drosophila* as a cell proliferation and tissue growth/size regulating pathway but now implicated in varied developmental/pathological paradigms [38]), which has emerged as an important means of correctly specifying the emerging blastocyst lineages. Specifically, that encapsulated and apolar inner-cells of the nascent ICM, generated after the 8- to 16- and 16- to 32-cell stage transitions, form active Hippo-signalling centres at adherens junctions (AJs) that potentiate the terminal core pathway kinases, LATS1/2 (in a mechanism requiring recruitment of the essential activator AMOT [39, 40, 41]) to phosphorylate the transcriptional cofactors effectors YAP and WWTR1/TAZ (collectively referred to here as YAP). Combined YAP phosphorylation (promoting cytoplasmic 14-3-3- proteins binding) and AMOT interaction prevents YAP nuclear accumulation that ensures members of the TEA-domain containing transcription factors (specifically TEAD4 in this context) are unable to activate TE-specific genes (*e.g. Cdx2* or *Gata3*) [40]. Conversely, AJ-localised Hippo-pathway activation at basolateral membranes of polarised outer-cells is actively suppressed via AMOT protein sequestration to the cell contactless apical pole permitting unphosphorylated YAP to enter the nucleus to molecularly endow TEAD4 to appropriately transcriptional activate TE-related gene expression. Therefore, the initial inheritance, or otherwise, of an apical pole enriched in apical polarity factors (*e.g.* aPKC-Par complex) defines whether dividing 8-cell (E2.5) or outer 16-cell (E3.0) stage progeny blastomeres, respectively suppress or activate Hippo-signalling and hence exhibit pluripotency (as an inner-cell) or initiate TE differentiation (as an outer-cell). Indeed, experimental strategies to disrupt outer-cell apical-basolateral polarity [42, 43, 44, 45], or abrogate *Tead4* expression [46, 47, 48], result in failed outer-cells TE specification and ectopic ICM pluripotency-related marker gene expression (reviewed [49, 50]). Interestingly, YAP enabled TEAD4 complexes simultaneously suppress pluripotent gene expression (*e.g. Sox2*) in derived outer-cells [51, 52] and prevent precocious *Sox2* expression prior to the 16-cell stage [53]. Additionally, experimentally activated Hippo-signalling (*i.e.* LATS1/2 over-expression, to antagonise YAP-TEAD4 formation) can potentiate *Sox2* expression (even in outer-cells) by the 32-cell/ early blastocyst stage [51]. However, eventual EPI specification by the late blastocyst stage, actually requires later YAP translocation into the nucleus, in a process that is inherently heterogeneous and leads to competitive apoptotic elimination of EPI progenitors exhibiting reduced naïve pluripotency-related gene expression (and low nuclear YAP) [54]. Collectively, these data illustrate the integral role of Hippo-signalling in regulating key cell fate events in early mouse embryogenesis and suggest potential functional roles for other, potentially novel, factors capable of interacting with core Hippo-pathway components.

132 The WW-domain and C2-domain containing (WWC-domain) protein KIBRA was originally identified as an
133 interactor of Dendrin, a modulator of post-synaptic cytoskeleton [55]. Subsequently, *Kibra* was reported as a positive
134 regulator of Hippo-signalling in *Drosophila* tumour suppressor/cell proliferation screens by phosphorylating the fly
135 orthologue of mammalian LATS1/2, *warts*/*Wts* [56, 57, 58]; subsequently confirmed by KIBRA-LATS1/2 interactions in
136 mammalian cells [59]. In contrast to *Drosophila*, tetrapod genomes typically encode three WWC-domain paralogs
137 (*KIBRA/WWC1*, *WWC2* and *WWC3*; *Mus musculus* genome only contains *Wwc1/Kibra*, hereon referred to as *Kibra*,
138 and *Wwc2* owing to evolutionarily recent chromosomal deletion of the ancestral *Wwc3*). Human KIBRA shares 49%
139 and 40% amino acid identity WWC2 and WWC3, respectively, and all paralogs are cable of homo- and hetero-
140 dimerisation (in all combinations). All three paralogs can also activate Hippo-signalling (causing LATS1/2 and YAP
141 phosphorylation) in inducible cell line models and cause the Hippo-related *Drosophila* 'rough-eye' phenotype, caused
142 by reduced cell proliferation, when over-expressed in the developing fly eye [60]. The WW-domain (found as N-
143 terminal tandem repeats in KIBRA and WWC2/3) is one of the smallest known protein domains, comprising 35
144 amino acids and interacts with short proline rich motifs (~4-6 amino acids) containing the consensus sequence,
145 L/PPxY [61]. Interestingly, WW-domains and L/PPxY-motifs are enriched in confirmed Hippo-signalling-related
146 proteins [61] and in potential regulator/effectors identified in comprehensive proteomic assays of the human Hippo-
147 pathway interactome [62]. Despite a comparatively large pan-model KIBRA-related Hippo-pathway activator literature,
148 the roles of WWC2/3 are understudied and restricted to limited reports consistent of tumour suppressor function in
149 specific cancers (*e.g.* hepatocellular carcinoma [63] and epithelial-mesenchymal lung cancers [64]). Therefore, due to the
150 importance of differential/regulated Hippo-signalling in early mouse development [49] and the collective paucity of
151 WWC-domain gene related data within this developmental window, we investigated the effect of dysregulating *Kibra*
152 and *Wwc2* expression in mouse preimplantation embryos.
153 We report specific disruption of *Wwc2* expression in mouse embryo blastomeres results in cell autonomous
154 division and cleavage phenotypes associated with mis-segregated chromosomes and defective cytokinesis (not
155 replicated by targeted dysregulation of *Kibra*). The collective defects yield blastocysts with fewer overall cells,
156 increased ICM apoptosis and reduced capacity to populate pluripotent EPI; indicating a potential pluripotency
157 regulating role. Observed phenotypes were rescued by the expression of epitope-tagged recombinant WWC2 protein,
158 that localised within the persistent mid-body structures between blastomeres post cleavage/division [65]. Furthermore,
159 we report similarly rescuable cell division phenotypes associated with impaired *Wwc2* expression in meiotically
160 maturating mouse primary oocytes, that are coincident with profound spindle defects and a block in
161 activating/phosphorylating the key cell-cycle regulatory kinase Aurora-A (AURKA). Accordingly, we conclude
162 *Wwc2* is a novel regulator of both female acentrosomal meiotic and early embryonic mitotic cell division and mouse
163 blastocyst cell fate.

164 **RESULTS**

165

166 **WWC-domain containing genes are expressed in preimplantation mouse embryos**

167 As introduced above, in the context of the central role of Hippo-signalling in mouse preimplantation embryo
168 development [49], we investigated the potential regulatory role of WWC-domain containing genes (*i.e. Kibra* and *Wwc2*
169 in mice [60]) in blastocyst formation. Accordingly, we first assayed *Kibra* and *Wwc2* mRNA expression in
170 preimplantation mouse embryos microinjected with non-specific control dsRNA or constructs specific for each gene
171 (Fig. 1a). Stable levels of *Kibra* and *Wwc2* transcripts were readily detectable at both 8- (E2.5) and 32-cell (E3.5)
172 stages, with normalised *Wwc2* expression twice as abundant as *Kibra*. Each transcript level could be robustly reduced
173 using dsRNA mediated global knockdown at both assayed stages (note, a lack of available antibodies prevented
174 protein expression assays). We next assayed for overt developmental defects associated with individual or combined
175 *Kibra*/*Wwc2* knockdown by microinjecting dsRNA(s) in one blastomere of 2-cell (E1.5) stage embryos, culturing to
176 the late blastocyst (E4.5) stage and counting total cell number (Fig. 1b). *Kibra* gene knockdown had no significant
177 effect on total cell number, or embryo morphology (versus control dsRNA), but a severe attenuation in cell number
178 when targeting *Kibra* and *Wwc2* transcripts in combination was observed. Interestingly, this defect was statistically
179 indistinguishable from the group of embryos microinjected with *Wwc2* dsRNA alone, indicating sole knockdown of
180 the *Wwc2* paralog was sufficient to induce the observed phenotype (note, *Kibra* mRNA levels were unaffected by
181 *Wwc2* dsRNA by the 8-cell/E2.5 stage, whereas *Wwc2* transcripts were robustly reduced, confirming *Wwc2* dsRNA
182 specificity – Fig. 1a and supplementary Fig. S1). Repetition of the *Wwc2* knockdown, in a fluorescently marked clone
183 (whereby rhodamine conjugated dextran beads/ RDBs were co-injected with *Wwc2* siRNA) confirmed reduced cell
184 numbers as early as the 16-cell (E3.0) stage, specifically within the marked clone that itself exhibited reduced
185 contribution to the initial inner-cell/ ICM founding population (Fig. 1c). Accordingly, we decided focus our further
186 investigations on the overt phenotype associated with *Wwc2* knockdown.

187

188 **Embryo cell number deficits caused by *Wwc2* knockdown are associated with defective cell division.**

189 Although the utilised *Wwc2* dsRNA was carefully designed to avoid off target effects (with specifc respect
190 to *Kibra* expression, Figs. 1a & S1), we sought to phenocopy our observations using an siRNA mediated approach
191 (targeting an alternative region of the *Wwc2* mRNA – Fig. S1); thus, providing added confidence to our initial
192 observations and affording the option of phenotypic rescue, by expressing recombinant siRNA-resistant *Wwc2*
193 mRNA. Figure 2 confirms the selected *Wwc2* siRNA near completely eliminated detectable *Wwc2* transcripts, after
194 global knockdown, in 32-cell (E3.5) stage blastocysts. Moreover, subsequent to the microinjected 2-cell (E1.5) stage,
195 an assay of total cell number at all cleavage stages up to the late blastocyst (E4.5) stage revealed an accumulative
196 and statistically robust deficit beginning after the 8-cell (E2.5) stage (Fig. 2c). Indeed, from the equivalent 8-cell
197 (E2.5) to 32-cell (E3.5) stages (judged by control embryo development), total cell number did not significantly
198 increase in *Wwc2* knockdown embryos but did start to increase during the blastocyst maturation period (32- to >64-
199 cell, as judged in control embryo groups; *i.e.* E3.5 – E4.5 stages). Significantly, it was not unusual for the *Wwc2*
200 knockdown embryos to initiate cavitation (not shown). We also assayed if the *Wwc2* siRNA phenotype was cell
201 autonomous by creating RDB marked *Wwc2* specific siRNA knockdown clones (comprising 50% of the embryo –
202 Fig. S2). As expected, we observed a statistically significant *Wwc2* siRNA mediated deficit in cell number within the

203 microinjected clone (versus the non-microinjected sister clones and the equivalent microinjected clone in control
204 siRNA embryos) at all stages, from the 8-cell (E2.5) to the late blastocyst (E4.5). However, we did not observe
205 significant differences between control and *Wwc2* knockdown groups in the number of cells within the non-
206 microinjected clone (with the exception of the 32-cell (E3.5) stage where there were an average of 2.3 fewer cells in
207 the *Wwc2* knockdown group). These data support a novel and cell autonomous role for *Wwc2* in regulating
208 appropriate cell number during preimplantation mouse embryo development. Whilst assaying cell numbers, we
209 observed a number of nuclear/chromatin morphological abnormalities within *Wwc2* knockdown embryos, not evident
210 in control embryos. Illustrative examples, at the equivalent of the 32-cell (E3.5) stage are provided (Fig. 3b) and were
211 categorised as; 'abnormal nuclear morphology' (including that typical of persistent 'association with the mid-body'),
212 associated with 'cytokinesis defects' (typified by bi-nucleated cells) or coincident with 'multiple or micronuclei'.
213 Accordingly, we calculated the frequencies by which each, or a composite of, the stated abnormalities were observed
214 (compared to control siRNA conditions) at each assayed cleavage stage; defined per embryo (in at least one
215 blastomere) or per individual assayed cell (Fig. 3c). Except from a single incidence of an early blastocyst stage cell
216 exhibiting a single micronucleus, no other abnormalities were observed in any control siRNA microinjected embryo,
217 at any developmental stage. Conversely, abnormally shaped nuclei were present in over a quarter of *Wwc2*
218 knockdown embryos at the 8-cell (E2.5) stage and were found in all assayed embryos by the equivalent late blastocyst
219 (E4.5) stage. A similar trend, from the 16-cell (E3.0) stage, was observed in relation to multiple/micronuclei. Despite
220 being less prevalent, cytokinetic defects affected nearly a quarter of *Wwc2* knockdown embryos by the late blastocyst
221 (E4.5) stage. Indeed, all *Wwc2* knockdown embryos exhibited one or more defect, in at least one cell, by the mid-
222 blastocyst (E4.0) stage, with the collective defects (excluding cytokinesis/bi-nucleation) first arising in just over a
223 quarter of 8-cell stage (E2.5) embryos. When we analysed the same phenotypes on the level of each individually
224 assayed blastomere, we found that just over a quarter of cells were affected by the late blastocyst (E4.5) stage;
225 however, it should be noted that such embryos comprised a much smaller average of overall cells, versus control
226 siRNA groups (*i.e.* 31.3±3.0 against 87.0±3.8 - Fig. 2c). Hence, our collective interpretation is *Wwc2* knockdown in
227 cleavage stage mouse embryos is associated with cell autonomous division defects that contribute to embryos with
228 progressively fewer constituent blastomeres as preimplantation development proceeds past the 8-cell stage; invoking
229 a role for *Wwc2* in regulating appropriate cell division/ mitosis in blastomeres of the early mouse embryo.
230
231 **siRNA mediated *Wwc2* knockdown affects blastocyst cell fate derivation.**
232 As described, cell number deficit/defective cell division phenotypes were first evident in global siRNA
233 mediated *Wwc2* knockdown embryos around the 8- to 16-cell stage (Figs. 2 & 3). Moreover, clonal dsRNA mediated
234 *Wwc2* knockdown analysis was specifically associated with reduced inner-cell clone numbers (Fig. 1c). As the
235 transition from the 8- to 16-cell stage, represents the first developmental point constituent embryonic cells are overtly
236 distinct, both in terms of intra-cellular apical-basolateral polarity and relative spatial allocation, with consequences
237 for ultimate blastocyst cell fate (*i.e.* comprising polarised outer-cells that can give rise to both TE and further inner-
238 cells, plus apolar inner ICM progenitors [66]), we assayed if clonal *Wwc2* knockdown altered TE versus ICM cell fate
239 by the early blastocyst (E3.5) stage. The need to assay the first cell fate decision, in this context, was further reinforced
240 by cited precedents implicating *Kibra,* and hence by association its paralog *Wwc2*, in activating Hippo-signalling in
241 flies and mammals [56, 57, 58, 59, 60], itself central to TE /ICM specification in mouse preimplantation embryos [49].

242 Accordingly, we created stably marked clones of *Wwc2* knockdown and control cells (by expressing recombinant
243 GAP43-GFP as an injection membrane marker) and assayed expression of the Hippo-sensitive TE marker protein
244 CDX2 [67] (Fig. 4). Control siRNA treated embryos developed appropriately to yield 32-cell (E3.5) stage blastocysts
245 consisting an average of 59% outer (CDX2 positive) and 41% inner (CDX2 negative) cell populations, with a
246 statistically equal contribution from each clone (*i.e.* either control siRNA microinjected or non-microinjected
247 derived). As expected, *Wwc2* siRNA microinjected embryos comprised significantly fewer cells with the
248 microinjected clone also characterised by the previously observed abnormal nuclear morphologies and a robustly
249 significant impaired contribution to the ICM; on average 1.6±0.2 cells versus 6.8±0.3 in the non-microinjected clone
250 (or 7.3±0.4 or 7.4±0.3 in the respective clones of control siRNA microinjected embryos). Clonal TE contribution was
251 also significantly impaired but to a much lesser degree and the potential TE deficit was compensated by an increased
252 contribution from the corresponding non-microinjected clone. We also observed a small outer-cell population of
253 *Wwc2* knockdown clones that failed to express CDX2 (~20%; not observed in control embryos) with the remaining
254 outer-cells often exhibiting comparatively reduced CDX2 immunoreactivity, when compared to both the non-
255 microinjected clone or either clone in the control siRNA microinjected groups (concurrently immuno-stained and
256 imaged using identical protocols; Fig. 4b). However, no ectopic CDX2 expression within inner-cells of the *Wwc2*
257 knockdown clone was observed and the non-microinjected clone appropriately only expressed CDX2 in outer-cells.
258 Therefore, consequent to clonal *Wwc2* knockdown, the overall percentage make up of outer and inner-cells was
259 skewed in favour of outer TE (largely CDX2 positive – 72%) over ICM (exclusively CDX2 negative - 28%). These
260 results suggest that the required outer-cell Hippo-pathway suppression (to specify TE) and inner-cell activity (to
261 prevent TE differentiation and promote pluripotency) are predominantly intact within the *Wwc2* knockdown clone,
262 although maintenance of TE specification/ differentiation in outer-cells is modestly impaired. Therefore, endogenous
263 *Wwc2* is unlikely to function as a centrally critical Hippo-signalling pathway (*i.e.* LATS1/2) regulator (as implied by
264 previous *Kibra/KIBRA* related reports demonstrating a role in Warts/LATS1/2 phosphorylation/activation in
265 *Drosophila* and mammalian cells [56, 57, 58, 59, 60]), in the specific context of TE versus ICM cell fate
266 specification/segregation, prior to blastocyst formation. Indeed, such conclusions are supported by a lack of overt
267 apical polarity (PARD6B) defects or ectopic nuclear exclusion of YAP (as the transcriptional co-activator and Hippo-
268 pathway effector protein [40]) in outer-residing *Wwc2* knockdown blastomeres, by the 32-cell (E3.5) stage (Fig. S3).
269 However, normal YAP nuclear exclusion in inner-residing *Wwc2* knockdown cells was found to be consistently less
270 robust than that observed in equivalent inner-cells of control siRNA microinjected embryos, possibly suggesting
271 moderately impaired Hippo-signalling activation/ cytoplasmic YAP sequestration caused by *Wwc2* knockdown (Fig.
272 S3); although the observed nuclear YAP levels were far from equivalent to those observed in outer residing
273 blastomeres of the same embryos (Fig. S3). Such data are indicative of a potentially mild inhibition of active Hippo-
274 signalling in such inner *Wwc2* knockdown cells, by the 32-cell (E3.5) stage.

275 We next extended the analyses to the late blastocyst (E4.5) stage cell lineages, assaying TE and EPI markers
276 (*i.e.* CDX2 & NANOG) or PrE and EPI markers (*i.e.* GATA4 & NANOG or GATA4 & SOX2) as pairwise
277 combinations (Figs. 5 & S4). We again observed *Wwc2* knockdown clone specific cell number deficits (relayed into
278 reduced total blastocyst cell number) and nuclear morphology/cell division related phenotypes. Despite such defects,
279 and contrasting with the early blastocyst stage, the ratio of total outer (TE) to inner (ICM) cells was not significantly
280 different between *Wwc2* or control siRNA microinjection groups (across all assayed lineage combinations; Fig. 5d-

281 f); indicating a degree of regulative development during blastocyst maturation. However, collectively we noted
282 incidences of fragmented nuclei, indicative of apoptotic cell death, that were significantly more prevalent within the
283 ICM of *Wwc2* siRNA, versus control siRNA, microinjected embryo groups. Moreover, the observed apoptosis was
284 significantly enriched within the microinjected clone of *Wwc2* knockdown embryos, suggesting such ICM residing
285 cell clones are prone to an increased probability of cell death (Fig. 5b). Consistently, the overall and significantly
286 reduced contributions of *Wwc2* siRNA derived clones were more pronounced for ICM versus outer-cell populations
287 (Fig. S4). Focussing, on CDX2 and NANOG immuno-stained groups, we again noted a population of CDX2 negative
288 outer-cells and generally reduced CDX2 expression within the *Wwc2* knockdown clone (Fig. 5c). Moreover, the
289 significantly reduced number of ICM cells derived from the *Wwc2* knockdown clone did not segregate between
290 NANOG positive (indicative of EPI) and NANOG negative (potentially PrE) cells, as per marked control siRNA
291 clones (*i.e.* according to a clone's overall percentage contribution within the ICM), but were significantly biased to
292 populate the potential, NANOG negative, PrE (Fig. 5d). Considering the embryos in the whole, the overall reduction
293 in size of the potential PrE (NANOG negative) population that was associated with clonal *Wwc2* knockdown, was
294 much less than that observed in the EPI (Fig. S4). This suggests inner *Wwc2* siRNA microinjection derived clones
295 are impaired in their contribution to sustain EPI numbers, by the late blastocyst (E4.5) stage, but are able to
296 differentiate to form PrE. This interpretation was supported by data directly assaying the two ICM lineages (*i.e.*
297 GATA4 in combination with either NANOG or SOX2; Figs. 5e & f, plus Fig. S4), whereby the characteristically low
298 number of inner *Wwc2* knockdown cells/clones observed, similarly segregated in a manner favouring the PrE (marked
299 by GATA4) over EPI (marked by either NANOG or SOX2); note, compensatory increases in EPI contribution were
300 also observed in the non-microinjected clone (Fig. S4). We also observed numerous examples of fragmented/
301 apoptotic inner-cell nuclei displaying distinct immuno-reactivity for SOX2 (Fig.5c), suggesting the increased
302 incidence of apoptosis observed within the ICM residing and microinjected cell clones of *Wwc2* knockdown embryos
303 (Fig. 5b) is centred on specified EPI that is ultimately unable to be maintained (although it was not possible to reliably
304 quantify the number of SOX2 positive apoptotic nuclei). Interestingly, in *Wwc2* siRNA microinjected embryo groups,
305 we also observed a small population of marked ICM clones that expressed neither PrE or EPI markers (comprising
306 4.6% of all ICM cells and 18.7% of the clone) that were not present in control siRNA treated groups, potentially
307 indicative of a further impairment in ICM cell fate derivation. In conclusion, our late blastocyst cell fate analyses
308 confirm *Wwc2* knockdown clone specific and autonomous reductions in overall cell number, that more robustly affect
309 the ICM versus TE. Such reductions are compensated for by regulation within the non-injected clone, that ultimately
310 preserves the overall TE:ICM ratio (albeit with fewer overall cells). However, the lineage contribution of *Wwc2*
311 knockdown clones within the ICM is biased against the pluripotent EPI in favour of PrE differentiation, via an
312 implicated mechanism possibly involving clone specific and selective EPI apoptosis; suggesting a role for *Wwc2* in
313 contributing to specified EPI maintenance that is additional to that related to cell division, yet inherently difficult to
314 experimentally resolve.
315

316 **siRNA resistant *HA-Wwc2* mRNA rescues *Wwc2* siRNA knockdown phenotypes; recombinant HA-WWC2**
317 **protein associates with cell division generated mid-bodies.**

318 Despite obtaining consistent RNAi phenotypes using distinct dsRNA/siRNA constructs and their careful
319 design aimed to avoid potential off-target effects or cross reactivity with paralogous *Kibra* mRNA (Figs. 1 and S1),

320 we sought to further verify the identified novel role of *Wwc2*. Accordingly, we derived a recombinant and N-
321 terminally HA-epitope tagged *Wwc2* mRNA construct (*HA-Wwc2*) that had been specifically mutated within the
322 siRNA complementary sequence (yet preserving a redundant sequence of amino acid codons; see Fig. S5) to block
323 recognition and hence remain available for translation in *Wwc2* siRNA containing cells. Thus, we repeated our
324 marked clonal microinjection experiments but added a third condition in which *Wwc2* siRNA was co-microinjected
325 with *HA-Wwc2* mRNA. Microinjected 2-cell (E1.5) stage embryos were cultured until the early (E3.5) and late (E4.5)
326 blastocyst stages and total/clonal cell contributions to inner/outer-cell populations, plus the incidence of abnormal
327 nuclear morphology, calculated (Fig. 6). Compared with the control siRNA group, embryos microinjected with *Wwc2*
328 siRNA alone exhibited the typical clone autonomous phenotypes described above. However, under *Wwc2* siRNA
329 conditions supplemented with co-microinjected *HA-Wwc2* mRNA (the expression of which was confirmed, see
330 below and Fig. 6d) the average number and clonal/spatial composition of constituent early (E3.5) and late (E4.5)
331 blastocyst cells was statistically indistinguishable from control siRNA microinjections groups (with the only
332 exception being a small reduction in the ICM contribution of the non-microinjected clone by the late/E4.5 blastocyst
333 stage; *i.e.* from 9.5±0.4 to 8.2±0.3). Additionally, there was a complete rescue of the incidence of nuclei with
334 abnormal morphology (with only one exception in all blastomeres assayed – shown in Fig. 6d). Collectively, these
335 data demonstrate the specificity of the RNAi reagents and confirm *Wwc2* as a novel regulatory gene of cell division
336 dynamics, with consequences for cell lineage derivation in preimplantation stage mouse embryo development. As
337 referenced above, the HA-epitope tag incorporated within the confirmed *HA-Wwc2* 'phenotypic rescue' mRNA
338 construct not only enabled us to verify its translation but also its sub-cellular localisation within the microinjected
339 clone, using an immuno-staining approach. Interestingly, given the clone autonomous cell number/division defects
340 observed after *Wwc2* knockdown, we consistently detected anti-HA immuno-reactivity at structures typical of mitotic
341 spindle derived mid-bodies (generated after cytokinesis), that were particularly evident within the *HA-Wwc2*
342 microinjected clones at the 32-cell stage (Fig. 6d & Fig. S6a). As a recent study identified a critical role for
343 uncharacteristically persistent interphase mid-bodies (referred to as 'interphase microtubule bridges') as important
344 MTOCs within the blastomeres of cleavage stage embryos [65], we assayed their number (immuno-staining for α-
345 Tubulin and activated phospho-Aurora-B/pAURKB, as recognised midbody markers – [68]) in control and *Wwc2*
346 knockdown embryos at the same 32-cell stage, but could not detect any statistically significant variation in their
347 overall incidence (when corrected for the reduced cell number caused by *Wwc2* knockdown - Fig. S6c-e). Hence
348 whilst *HA-Wwc2* derived recombinant protein is associated with cell division mid-bodies, the removal of endogenous
349 *Wwc2* mRNA does not appear to impair mid-body formation or persistence following compromised cell division.
350

351 ***Wwc2* mRNA depletion in primary (GV) oocytes impairs meiotic maturation.**

352 We next asked the question whether a similar knockdown of *Wwc2* expression in meiosis I arrested germinal
353 vesicle (GV) stage primary mouse oocytes would elicit any defects during maturation to the metaphase arrested stage
354 of meiosis II (MII), particularly because both paradigms of cell division occur in the absence of centrioles [5, 6, 8, 9, 10,
355 11, 22]. We observed abundant *Wwc2* transcripts in GV and MII oocytes (plus zygotes) that show evidence of becoming
356 cytoplasmically poly-adenylated, and hence more likely to be translated as required functional proteins [69], between
357 the GV and MII stages (as revealed using alternative, oligo-dT versus random hexamer, cDNA synthesis priming
358 strategies - Fig. 7a); indeed consultation of our previously published assay of meiotically maturing oocyte polysome

359 associated transcripts [70] supports this interpretation (~40% polysome association; Fig. 7b). We therefore confirmed
360 our *Wwc2* siRNA construct could elicit robust knockdown in microinjected GV oocytes, that had been blocked from
361 re-entering meiosis I (using a cAMP/cGMP phosphodiesterase inhibitor, 3-isobutyl-1-methylxanthine/ IMBX) and
362 then permitted them to *in vitro* mature (IVM) to the MII equivalent stage (Fig. 7c & d). Such oocytes were fixed and
363 immuno-fluorescently stained for α-Tubulin (plus DAPI DNA stain), to assay for potential phenotypes. In our two
364 control conditions (*i.e.* non-microinjected or control siRNA microinjected oocytes) >90% of GV oocytes matured to
365 the MII arrested stage, typified by an extruded polar body (PB1) and metaphase II arrested spindle. However, in the
366 *Wwc2* knockdown group the successful IVM rate was reduced to 8.6% and oocytes presented with various arrested
367 phenotypes (lacking PB1) that we categorised by the presence of metaphase I meiotic spindles (-PB1 +MI spindle;
368 42.9% - note such spindles typically failed to migrate to the oocyte cortex), a spindle-like structures with mis-aligned
369 or dispersed chromosomes (-PB1 +spindle defect; 22.9%) or a non-nuclear membrane enveloped ball of chromatin
370 (-PB1+ultra-condensed chromatin; 25.7%), collectively indicative of severely impaired segregation of bivalent
371 chromosomes in a defective meiosis I (Fig. 7e). Despite, permitting assayed GV oocytes to meiotically mature for 18
372 hours, we wanted to confirm if the observed *Wwc2* knockdown phenotypes would persist or resolve if provided with
373 increased time (possibly indicative of delayed rather than blocked meiotic progression). We repeated the *Wwc2*
374 knockdown experiment allowing an extended IVM period of 24 hours. However, no increased frequency of MII
375 arrested oocyte generation was observed; rather *Wwc2* mRNA depleted oocytes either remained blocked in meiosis
376 I or unsuccessfully attempted to segregate their chromosomes, without undergoing cytokinesis (Fig. S7).
377
378 ***Wwc2* specific oocyte meiotic maturation phenotypes are associated with failed Aurora kinase-A (AURKA)**
379 **activation.**
380 It is reported that activated/phosphorylated Aurora kinase-A (p-AURKA: p-Thr288) is required to initiate
381 acentriolar/ MTOC mediated spindle assembly in mouse oocytes and that *Aurka* knockdown phenotypes resemble
382 those observed here for *Wwc2* knockdown [21]. We therefore hypothesised the meiotic maturation phenotypes identified
383 in *Wwc2* mRNA depleted GV oocytes may be associated with impaired levels of activated p-AURKA. A western blot
384 analysis of staged maturing oocytes confirmed characteristically low levels of p-AURKA in GV oocytes, that robustly
385 increased with the appearance of the first meiotic spindle (during MI) and were maintained with the formation of the
386 second meiotic spindle (in MII arrest; Fig. 8b & [15, 16]); a trend replicated in control siRNA microinjected GV (assayed
387 after 18 hour incubation in IMBX) and MII (after 18 hours post-IBMX removal) oocytes (note, the specificity of the
388 anti-p-AURKA antibody used was additionally confirmed; Fig. S8). However, in the *Wwc2* siRNA microinjected
389 group, we were not able to detect p-AURKA at either the equivalent GV or MII stages. Moreover, we were also
390 unable to detect p-AURKA immuno-reactivity localised to the poles of any spindles or spindle-like structures formed
391 in *Wwc2* knockdown oocytes, in stark contrast to that observed on MII arrested spindles in controls (Fig. 8c);
392 confirming a failure to activate AURKA under conditions associated with profound meiotic oocyte maturation
393 defects. We next employed the *HA-Wwc2* rescue mRNA construct in an attempt to reverse the observed *Wwc2*
394 knockdown oocyte maturation phenotypes. Using a similar IVM assay (but assaying at multiple time-points), we
395 found that co-microinjection of *HA-Wwc2* mRNA and *Wwc2* siRNA was able to robustly rescue the maturation
396 phenotypes caused by *Wwc2* siRNA microinjection alone (*i.e.* MII arrested oocytes at 16 hours post-IBMX; control
397 siRNA – 81.8%, *Wwc2* siRNA - 8.7% & *HA-Wwc2* mRNA plus *Wwc2* siRNA – 76.0%); moreover the progression

398 of the rescue through recognisable maturation stages was in-step with that of control siRNA microinjected oocytes
399 (as measured at 1, 6 , 12 and 16 hours post-IBMX removal; Fig. 8d). Consistently we also found co-microinjection
400 of the rescue *HA-Wwc2* mRNA construct was coincident with reappearance of activated p-AURKA protein (Fig. 8e),
401 that was also detected in proximity to forming or matured MI/MII stage meiotic spindles (Fig. S9). Collectively, these
402 data confirm a novel role for *Wwc2* in regulating appropriate bivalent chromosome segregation during mouse primary
403 oocyte meiotic maturation that is strongly associated with activation of the acentriolar/MTOC mediated spindle
404 forming meiotic/ mitotic kinase AURKA.

405 **DISCUSSION**

406

407 In the current study, we have identified *Wwc2*, the sole murine WWC-domain containing paralog of the
408 recognised Hippo-pathway activator *Kibra* [56, 57, 58, 59, 60], as a novel mitotic regulator of preimplantation mouse embryo
409 cell cleavage divisions (Figs. 1-3); plus a similar role in primary mouse oocyte meiotic maturation (Fig. 7), predicated
410 on appropriate activation/phosphorylation of the cell-cycle kinase AURKA (Figs. 8 and S9). Additionally, we have
411 shown *Wwc2* knockdown cell clones are compromised in ultimately contributing to the specified EPI lineage, by the
412 late blastocyst stage, being prone to apoptosis or disproportionate contribution to PrE (Figs. 5 and S4). Thus,
413 collectively these data implicate at least two functional roles for *Wwc2* during early mouse
414 development/reproduction; i) spatial and temporal regulation of correct cell division spindle apparatus formation and
415 function in both meiotic primary oocytes or early mitotic embryonic blastomeres (each paradigms of typical and
416 atypical, acentrosomal/acentriolar cell division, relative to other mammalian species, respectively [5, 6, 8, 9, 10, 11]), and
417 ii) affecting individual blastomere pluripotency and differentiation, particularly with respect to EPI and PrE
418 derivation in the ICM of late mouse blastocysts (E4.5) (Figs. 5 and S4); however, the full extent of such a cell fate
419 related role, remains difficult to experimentally dissect, given the described cell division defects evident as early as
420 the 8-cell (E2.5) stage after *Wwc2* knockdown.

421 Relating to cell fate regulation, the attainment of naïve pluripotency within specified EPI cells of the late
422 (E4.5) mouse blastocyst has recently been shown to be regulated via a heterogeneous mechanism of activated
423 TEAD1-mediated transcription (caused by YAP relocalisation from the cytoplasm to the nucleus), that promotes
424 ICM cell/EPI progenitor competition and elimination (by apoptosis) [54]. This contrasts with earlier specification and
425 segregation of outer TE from founder ICM populations, prior to the blastocyst stage, whereby activated Hippo-
426 signalling and YAP nuclear exclusion is required for inner-cells to actively retain pluripotency (*e.g.* express *Sox2*)
427 and resist TE differentiation [49]. Hence, active Hippo-signalling seems to both support initial pluripotency in ICM
428 founders (*i.e.* confirmed - see [49]) but presumably needs to be suppressed in EPI progenitors to promote naïve
429 pluripotency (*i.e.* to permit nuclear YAP translocation, inferred from [54]). Our data, although compounded by the
430 additional cell division phenotypes, suggests *Wwc2* (as a paralog of the Hippo-activator *Kibra*) also contributes to
431 germane Hippo-signalling regulation. For example, relating to late blastocyst (E4.5) stage EPI specification, we find
432 ICM-residing *Wwc2* knockdown clones, although fewer than their non-microinjected clone counterparts, do not
433 display the same equal contribution to populate the EPI (NANOG+/SOX2+) and PrE (GATA4+) as observed in the
434 non-specific siRNA microinjected clones of control embryos (Figs. 5 and S4). Indeed, such clones statistically favour
435 PrE over EPI contribution, indicative of compromised pluripotent potential. Whether this is due to compromised
436 Hippo-signalling activation after initial internalisation prior to blastocyst formation, and/or relates to relative fitness
437 deficiencies affecting their ability to successfully compete to colonise specified EPI, is uncertain. However, an
438 increased apoptotic ICM cell number within *Wwc2* knockdown clones, often marked by detectable SOX2 protein
439 expression (but never GATA4 immunofluorescence), observed in late (E4.5) blastocysts (Fig. 5b & c) is consistent
440 with their competitive elimination. Although, the possibility remains the apparent lack of EPI fitness, associated with
441 *Wwc2* knockdown, is caused by an initial pluripotency deficit in ICM founders. Nevertheless, our analysis of early
442 stage (E3.5) clonal *Wwc2* knockdown blastocysts, suggests the establishment of differential Hippo-signalling
443 between TE (*i.e.* suppression) and ICM (*i.e.* activation) was largely intact (Figs. 4 and S3; *i.e.* CDX2, PARD6B,

444 CDH1 and YAP immuno-fluorescent staining). Although, the comparatively reduced (or sometimes absent)
445 expression of outer-cell CDX2 protein, plus less efficient YAP protein nuclear exclusion in inner-cells, in *Wwc2*
446 knockdown clones (compared with sister non-microinjected clones within the same embryo or non-specific siRNA
447 microinjected clones in control embryos; Figs. 4 and S3) implies some degree of mild early onset mild Hippo-
448 signalling defect; potentially becoming more manifest/relevant during blastocyst maturation/EPI specification. The
449 relatively mild early cell fate effects may also reflect functional redundancy between WWC2 and KIBRA, whereby
450 potential major Hippo-signalling defects caused by specific *Wwc2* knockdown are compensated by continued and
451 sufficient expression of *Kibra*; indeed, we demonstrated robust *Wwc2* knockdown does not affect *Kibra* mRNA levels
452 (Fig. 1 and S1). Support for functional redundancy between WWC-domain proteins paralogs has been demonstrated
453 in human cells (relating to KIBRA, WWC2 and WWC3 [60]) and genetic ablation of the mouse *Kibra* gene is
454 developmentally viable (with adult mice only exhibiting learning and memory deficits [71]). Interestingly, our initial
455 clonal dsRNA mediated knockdown of *Kibra* and *Wwc2* expression, either in isolation or combination (Fig.1),
456 demonstrated robust down-regulation of *Kibra* alone did not impair formation of cavitated late (E4.5) blastocysts
457 (comprising equal cell numbers to control dsRNA groups), suggesting loss of the *Kibra* paralog could be tolerated,
458 potentially due to continued *Wwc2* expression. However, sole *Wwc2* knockdown caused the profound defects present
459 in this study, despite continued expression of *Kibra,* and were not exacerbated by co-down regulation of *Kibra*.
460 Hence, if KIBRA and WWC2 proteins share functional redundancy during mouse preimplantation development, it
461 is likely only in relation to Hippo-signalling regulation and not applicable to the described cell division roles of
462 WWC2.

463 As described, siRNA mediated *Wwc2* knockdown causes cell autonomous deficits in total preimplantation
464 mouse embryo cell number (particularly affecting inner-cell populations), by the 16-cell (E3.0) stage (Figs. 2, 3 and
465 S2). Why reduced embryo cell numbers are manifest comparatively late, given initial microinjection is performed 2-
466 cell (E1.5) stage embryos is unclear. Possibly, all subsequent cell-cycles in *Wwc2* knockdown clones are elongated
467 in a manner that is only revealed on the whole embryo level by the 16-cell (E3.0) stage, implicating *Wwc2* as a
468 regulator of the atypically long cell-cycles of preimplantation mouse/mammalian embryo blastomeres (reviewed [37]).
469 Alternatively, it may reflect the developmental point maternally provided WWC2 protein, unaffected by siRNA, is
470 functionally depleted. However, it impossible here to directly probe WWC2 protein expression, due to a lack of
471 available antibodies. Although, we did confirm the abundant presence of poly-adenylated maternal *Wwc2* mRNAs
472 in both primary (associated with translating polysomes) and secondary mouse oocytes and zygotes (Fig. 7a & b), that
473 coupled with the functional role in meiotic maturation (Figs. 7, 8, S7 and S9), strongly suggest maternal WWC2
474 protein inheritance in early cleavage stage embryos. The appearance of cell number deficits from the 16-cell (E3.0)
475 stage also coincides with the first spatial segregation of blastomeres (*i.e.* outer- and inner- positions) and
476 polarity/position dependant differential Hippo-signalling establishment and TE versus ICM cell fate derivation [49]. As
477 *Wwc2* is a paralog of the confirmed Hippo-activator *Kibra* [56, 57, 58, 59, 60], it is tempting to speculate the developmental
478 timing of the cell number phenotype is particularly relevant. However, our experimental data suggest Hippo-
479 signalling at this time (*i.e.* prior to blastocyst formation) is at most mildly affected by *Wwc2* knockdown.
480 Additionally, the onset of individual nuclear morphological phenotypes, indicative of defective cell
481 division/cytokinesis (*e.g.* mid-body association, bi-/multi-/micro-nucleation; Fig. 3), were already evident by the 8-
482 cell (E2.5) stage. Moreover, whilst average cell number was impaired in *Wwc2* knockdown embryos after the 8-cell

483 (E2.5) stage, it did not significantly increase again until the mid-blastocyst (E4.0) stage (remaining around 8-10 cells
484 after global *Wwc2* knockdown, through the 16-/32-cell, E3.0/E3.5, stage equivalents; Fig. 2). This is significant as
485 the mid-blastocyst (E4.0) stage reflects the developmental point at which the atypically acentrosomal/acentriolar cell
486 cleavage divisions of mouse embryos, in comparison with most other mammalian species, reverts back to
487 centrosomal control, after *de novo* centrosomes synthesis [11] (although it could also reflect the waning effect of *Wwc2*
488 specific siRNA). Therefore, we propose our data demonstrate a role for WWC2 in regulating acentrosomal cell
489 division in preimplantation stage mouse blastomeres, prior to the mid-blastocyst (E4.0) stage. Moreover, that WWC2
490 is a regulator of mitotic spindle formation/functional dynamics, as reflected in phenotypic nuclear morphologies
491 observed after *Wwc2* knockdown (Fig. 3). Supporting this hypothesis, we readily detected recombinant HA-WWC2
492 protein (derived from microinjected siRNA resistant recombinant mRNA, used to successfully elicit phenotypic
493 rescue of *Wwc2* knockdown phenotypes – Figs. 6 and S5) in confirmed mitotic mid-bodies up until the early
494 blastocyst (E3.5) stage but much less easily by the late blastocyst (E4.5) stage (Figs. 6 and S6); *i.e.* subsequent to *de*
495 *novo* centrosome synthesis [11]. The hypothesis is further substantiated by our data relating to primary oocyte
496 maturation, in which GV stage oocytes depleted of *Wwc2* transcripts are unable, again in the absence of centrosomes
497 [5, 6, 8, 9, 10], to complete meiosis I and present with multiple spindle defects associated with failed
498 activation/phosphorylation of the key cell-cycle kinase, AURKA (Figs. 7, 8, S7 and S9). The importance of AURK
499 activity during early mouse embryo cell cleavage has been reported, whereby clonal siRNA mediated downregulation
500 of *Aurkb* and *Aurkc* expression respectively increases or decreases the rate of mitotic cell division (*Aurkb* and *Aurkc*
501 over-expression exhibit the opposing effects). Indeed, the reported cell number deficits associated with *Aurkc* down
502 regulation, strongly resemble those related to *Wwc2.* Increased *AurkC* expression was also shown to potentiate
503 pluripotent gene expression, whilst enhanced *Aurkb* expression impaired nuclear retention of recombinant photo-
504 activatable-OCT4 reporter protein [14]. It will be interesting to functionally probe any potential link between WWC2
505 and AURKB/AURKC, in the context of regulating pluripotency and Hippo-pathway regulation, in future studies.
506 The first report to implicate WWC-domain containing proteins in mammalian Hippo-signalling,
507 demonstrated human KIBRA (in HEK293T cells) binding to, and stimulating the phosphorylation/activation, of
508 LATS1/2, leading to subsequent phosphorylation of YAP [59]. The same authors later described mitosis specific
509 KIBRA phosphorylation, catalysed by AURKA and/or AURKB at a highly conserved AURK consensus/target motif
510 (centred on Ser539), that could be antagonised by the mitotic phosphatase PP1. Moreover, they reported over-
511 expression of a KIBRA mutant (S539A), promotes precocious M-phase exit in a model of SAC arrest, despite
512 continued activation of cyclin dependent kinase, CDK1 [72]. Thus, implicating KIBRA as an important molecular
513 component of M-phase progression/dynamics. Subsequently, the same group demonstrated KIBRA is required to
514 fully activate/phosphorylate AURKA, that in turn phosphorylates/activates LATS2, ensuring its appropriate
515 centrosomal localisation. Moreover, that siRNA mediated *KIBRA* transcript knockdown caused profound spindle
516 defects, lagging chromosomes and micronuclei formation, reminiscent of *Wwc2* knockdown-related phenotypes, plus
517 centrosomal fragmentation in human MCF7 and HeLa cell line models [73]; typical of direct LATS2 disruption, itself
518 known to promote centrosomal structural integrity [74] and accumulation of gamma-tubulin required for initiating
519 mitotic spindle assembly [75]. Interestingly, we have now confirmed the presence of the same AURK consensus motifs
520 in both murine KIBRA and WWC2 proteins (Fig. S10). Therefore, it is tempting to speculate the *Wwc2* knockdown
521 phenotypes we observe in preimplantation stage mouse embryos may be mechanistically related to those previously

522 described for human KIBRA, although with the caveat they function on the level of MTOC regulation, in the absence
523 of centrosomes/centrioles [11]. For example, targeted genetic ablations of the *Lats1* and *Lats2* genes in mice are not
524 described in association with the preimplantation embryo cell division/cell number deficits typical of *Wwc2*
525 knockdown, nor those described phenotypes above in relation to other models of mitosis. Rather, *Lats1*$^{-/-}$/*Lats2*$^{-/-}$
526 early blastocysts (E3.5) only present with ectopic nuclear YAP expression within ICM cells [40]. Therefore, not all
527 insights will be directly transferable. However, despite the lack of centrosomes in pre-mid-blastocyst stage mouse
528 embryos, classical key centrosome regulators are expressed and been shown to have functional cell division roles.
529 For example, genetic knockout of the M-phase cell-cycle regulator, Polo-like kinase 1 (*Plk1*), known to cooperate
530 with AURKA within centrosomes to mediated bi-polar spindle formation [76], interestingly arrests at the same 8-cell
531 (E2.5) developmental stage at which embryos subject to global *Wwc2* knockdown first present with cell division
532 defects (Figs. 2 and 3) [77]. Moreover, a critical role for the related *Plk4* gene, itself recognised as a key regulator of
533 centriole formation/duplication [78, 79], has been demonstrated during acentrosomal mouse blastomere division.
534 Accordingly, active PLK4 protein localises within the coalescing MTOCs forming around condensed chromatin and
535 in cooperation with the centrosomal protein CEP152, promotes microtubule nucleation and bi-polar spindle
536 formation and experimental depletion of active PLK4 results in the formation of mono-polar microtubule asters [22].
537 Hence, it will be interesting to further investigate the identified role of *Wwc2* during early embryo acentrosomal cell
538 division, through the prism of such pre-existing characterised, and MTOC-related/regulating, molecular components.
539 Furthermore, to test applicability of such potentially identified mechanisms within the conceptually similar paradigm
540 of acentrosomal meiotic divisions of the maturing primary oocyte (also identified here as under control of *Wwc2*).
541 Indeed, a role for PLK4 in mediating acentriolar spindle assembly in mouse oocytes, was recently described, whereby
542 MTOC resident PLK4, in cooperation with AURKA, participates in initiating microtubule nucleation around
543 condensing chromosome bivalents upon meiosis re-entry. However, unlike in mitotic blastomeres, functional
544 inhibition of PLK4 does not completely block bi-polar spindle formation but rather extends assembly completion
545 time. Moreover, the oocyte MTOC related roles of PLK4 and AURKA are only partially overlapping, with AURKA
546 contribution appearing to be dominant (*e.g.* catalytically targeting the microtubule minus end stabiliser TACC3) [21].
547 Interestingly, the identified MTOC mediated spindle formation role of PLK4/AURKA is distinct from the co-existing
548 mechanism of chromosome derived RAN-GTP gradient driven microtubule stabilisation in oocytes (as reviewed [5, 6,
549 8, 9, 10]). Clearly, in the context of *Wwc2* knockdown oocyte maturation phenotypes described here (that include failed
550 AURKA phosphorylation/activation), potential links between described PLK4/AURKA phenotypes and WWC2
551 merit further investigation. They are also consistent with reports implicating AURKA in the regulation of MTOC
552 dynamics and microtubule spindle nucleation [15, 17, 18, 19]. However, importantly the described inhibition of PLK4 was
553 associated with eventual polar body formation [21], unlike after *Wwc2* knockdown (even after an extended IVM
554 incubation time – Fig. S7), indicating that whilst meiotic spindle assembly is affected/impaired by *Wwc2* knockdown
555 (illustrated by a 25.7% incidence of spindle formation failure and a further 22.9% of oocytes exhibiting defective
556 spindles - Fig. 7e), other impediments to successful meiotic maturation must exist (potentially relating, although not
557 necessarily limited, to spindle migration, SAC, cytokines *etc.*). The comparative spread of observed meiotic
558 maturation failure phenotypes associated with *Wwc2* knockdown (*i.e.* failed spindle formation, defective spindles or
559 persistent/ non-dividing MI spindles – Fig. 7e) also suggests a degree of functional redundancy may exist in response

560 to loss of WWC2 protein; for example, potentially related to the compensatory abilities of three expressed AURK
561 paralogs (*i.e. Aurka*, *Aurkb* and *Aurkc*), as demonstrated in combinatorial genetic ablations in mouse oocytes [17].
562 In conclusion, we have identified the ill-characterised WWC-domain containing mouse gene *Wwc2* as an
563 important cell-cycle regulator in both preimplantation mouse embryo blastomeres and maturing primary oocytes;
564 both paradigms of acentrosomal cell division. Additionally, we have uncovered evidence for *Wwc2,* as a paralog of
565 the classically described Hippo-signalling activator *Kibra*, in participating in cell fate regulation in regard to
566 blastocyst ICM pluripotency. Despite the compounding nature of the two identified *Wwc2* knockdown phenotypes,
567 it will be of great interest to experimentally determine the key molecular interactions and further understand the novel
568 roles played by WWC2 protein, in both mouse preimplantation embryo cell fate and mitosis and maturing primary
569 oocyte meiosis.

570 **METHODS**

571

572 Mouse/mouse embryo related experimental procedures were approved and licensed by the local ethics
573 committee of the Biology Centre (in České Budějovice) of the Czech Academy of Sciences and by the responsible
574 committee of the Czech Academy of Sciences at the national level, in accordance with Czech and European Union
575 law.

576

577 **Embryo and oocyte culture and microinjection.**

578 2-cell stage (E1.5) embryo collection, from super-ovulated and mated 10 week old F1 hybrid (C57Bl6 x
579 CBA/W) female mice, and *in vitro* culture in mineral oil covered drops (~20 μL/ ~15 embryos) of commercial KSOM
580 (EmbryoMax® KSOM without Phenol Red; Merck, MR-020P-5F), was conducted as previously described [48].
581 Germinal vesicle (GV) stage primary oocytes were mechanically recovered from mature Graafian follicles of
582 dissected ovaries of dams after PMSG (pregnant mare serum gonadotrophin) hormone stimulation (7.5U
583 intraperitoneal injection of F1 hybrid strain, 48 hours prior). Recovered oocytes were placed into pre-warmed (37°C)
584 drops (~20 μl/ ~15 oocytes) of commercial CZB media (EmbryoMax® CZB media with Phenol Red; Merck, MR-
585 019-D) containing 100 μM IBMX (3-isobutyl-1-methylxanthine, a cAMP/cGMP phosphodiesterase inhibitor that
586 maintains GV meiosis I arrest), overlaid with mineral oil and incubated (37°C/ 5% CO_2) for 2 hours prior to
587 microinjection.

588 Individual blastomere dsRNA, siRNA or recombinant mRNA microinjections (or combinations thereof), plus
589 post-microinjection culture protocols, were performed on 2-cell stage embryos (in either one or both blastomeres)
590 according to defined protocols [80], using apparatus formerly described [48]. Recovered GV staged oocytes were
591 microinjected using a minimally adapted protocol; namely oocytes were microinjected on 37°C heated stage in
592 concaved glass microscope slides filled with CZB media (+ IBMX inhibitor, 100 μM), overlaid with mineral oil.
593 Post-microinjection, GV oocytes were returned to the incubator for another 18 hours (to permit microinjected siRNA
594 mediated gene knockdown or mRNA expression; CZB +IBMX media) then transferred to fresh/pre-equilibrated CZB
595 media drops lacking IBMX, to induce resumption of meiosis I and *in vitro* maturation. Cultured (and microinjected)
596 embryos and oocytes were assayed at various developmental points, as dictated by individual experiments. As
597 indicated, rhodamine-conjugated dextran beads (RDBs; 1 μg/ μl – ThermoFisher Scientific, D1818) were co-
598 microinjected to confirm successful blastomere/oocyte microinjection; a summary of the origin and concentrations
599 of all microinjected RNA species is given in supplementary methods tables SM1. Non-microinjected embryos, or
600 oocytes, (2-3 per microinjection experiment, per plate) served as culture sentinels to confirm successful *in vitro*
601 embryo development/oocyte maturation. In cases of AURKA chemical inhibition (to confirm specifity of anti-p-
602 AURKA antisera – Fig. S8), recovered GV oocytes were transferred from IMBX containing CZB media to pre-
603 equilibrated CZB media drops lacking IBMX but containing the specific AURKA inhibitor, MLN8237 (1μM;
604 Selleckchem, S1133).

605

606 **dsRNA and recombinant mRNA synthesis.**

607 Specific long dsRNA molecules targeting coding regions of mouse *Kibra* and *Wwc2* derived transcripts
608 (plus negative control GFP) were designed (and *in silico* validated using online E-RNAi resource [81]) and synthesised.

509 Briefly, gene specific PCR primer pairs, incorporating 5'- T7-derived RNA polymerase promoters and spanning
510 designed dsRNA complementary sequence, were used to derive *in vitro* transcription (IVM) template, using mouse
511 blastocyst (E3.5) cDNA as a template (or plasmid DNA for GFP). After agarose gel verification, the double stranded
512 DNA templates were used in preparatory IVM reactions, incorporating DNaseI and single-stranded RNase treatment
513 (MEGAscript T7; ThermoFisher Scientific, AMB13345), to generate dsRNA. The integrity of derived *Kibra*-,
514 *Wwc2*- and *GFP*-dsRNAs was confirmed by non-denaturing gel electrophoresis and quantified (Nanodrop). The PCR
515 primer sequences used are provided in supplementary methods table SM2.
516 Microinjected mRNA constructs were derived using commercially available IVT reaction kit (mMACHINE
517 T3; ThermoFisher Scientific, AM1348), in which restriction enzyme linearized (using *SfiI*) plasmid DNA was used
518 as template (2 µg) as follows; i. C-terminal GFP-fusion *Gap43* mRNA plasma membrane marker, from pRN3P-C-
519 term-GFP-Gap43 [82]), ii. C-terminal RFP-fusion histone H2B mRNA (from pRN3-C-term-RFP-Hist1h2bb, derived
520 in this study) and iii. siRNA-resistant N-terminal HA-tagged *Wwc2* mRNA (from pRN3P-N-term-HA-siRNAres-
521 Wwc2, derived here). All synthesised mRNAs were subject to post-synthesis 3' poly-adenylation tailing (Poly(A)
522 Tailing Kit - ThermoFisher Scientific, AM1350), confirmed by denaturing gel electrophoresis and quantified
523 (Nanodrop).
524
525 **Recombinant plasmid construct generation.**
526 Four recombinant plasmids (required for IVT) were generated, using standard molecular biological
527 protocols. RFP-histone H2B fusion protein (pRN3-C-term-RFP-Hist1h2bb) were derived by in frame cloning of a
528 high-fidelity PCR amplified cDNA (using Phusion® DNA polymerase, New England BioLabs, M05305) encoding
529 histone H2B (*Hist1h2bb,* lacking endogenous start and stop codons), flanked by oligonucleotide introduced
530 restriction sites (*NheI*), into the RNA transcription cassette plasmid pRN3-insert-RFP variant (vector encodes
531 required start and stop codons). Thus, generating required H2B-RFP fusion reporter, downstream of vector encoded
532 T3 RNA polymerase promoter (for IVT) and flanked by UTRs from the frog β-globin gene [83]. The IVT plasmid
533 encoding the siRNA-resistant N-terminal HA-tagged *Wwc2* mRNA (pRN3P-N-term-HA-siRNAres-Wwc2) was
534 created from an annotated full-length Riken mouse *Wwc2* cDNA clone (clone ID: M5C1098O04, Source Bioscience)
535 by deriving a high fidelity PCR product, with oligo introduced 5' (*SpeI*) and 3' (*NotI*) restriction sites and an in frame
536 N-terminal HA-epitope tag, and 'TA cloned' (after addition of 3' adenine nucleotide overhangs) it into pGEM®-T-
537 Easy plasmid vector (Promega, A1360). The derived plasmid was site mutagenesised (commercial service; EuroFins)
538 to alter the nucleotide (but not amino acid codon) sequence of the siRNA (utilised in this study) recognition motif;
539 details in supplementary figure S5. The recombinant gene sequence was sub-cloned, using introduced *SpeI* and *NotI*
540 restriction sites, into the multiple cloning site of the RNA transcription cassette plasmid pRN3P [80] to derive IVT
541 competent pRN3P-N-term-HA-siRNAres-Wwc2. All four derived plasmids were sequence verified and the PCR
542 primers (or relevant details) used to generate the required inserts are described in supplementary methods table SM3.
543
544 **Q-RT-PCR**
545 Per experimental condition, total RNA was extracted from ~30 (microinjected) mouse embryos (oocytes) *in*
546 *vitro* cultured to the desired developmental stage, using PicoPure RNA isolation kit (Arcturus Biosciences/
547 ThermoFisher Scientific, KIT0204), as instructed. Eluted RNA (10 µL) was DNaseI treated (DNA-*free* kit;

ThermoFisher Scientific, AM1906) and used to derive cDNA (30 µL), either via oligo-dT (embryos and oocyte) or random hexamer (oocytes only) priming (Superscript-III Reverse Transcriptase; ThermoFisher Scientific, 18080085). 0.5 µl of diluted template cDNA (1:3, nuclease-free water) per real-time PCR reaction (10 µl – SYBR Green PCR kit, Qiagen, 204143) was used to assay specific transcript abundance (CFX96 Real-Time System, BioRad). *Kibra* and *Wwc2* transcript levels were internally normalised against those for *Tbp* (TATA-binding protein) housekeeping gene and fold changes (±s.e.m.) derived using the ΔΔCt method [84]. A minimum of two biological replicates of at least three technical replicates were employed; specific gene oligo primer sequences (final reaction conc. 400 nM) are in supplementary methods table SM4.

Immuno-fluorescent staining and confocal microscopy imaging.

In vitro cultured (microinjected) embryos/oocytes were fixed (at required developmental stages) with 4% para-formaldehyde, immuno-fluorescently stained and imaged in complete z-series by confocal microscopy (using the FV10i confocal microscope, Olympus) as previously described [48]; supplementary methods table SM5 summarises the identity and combinations (plus employed concentrations) of primary and fluorescently conjugated secondary antibodies used. Additionally, the majority of immuno-fluorescently stained embryos/oocytes were counterstained for DNA, using DAPI containing mounting solution (Vectashield plus DAPI, Vector Labs) and as indicated some embryo samples were also counterstained against filamentous-actin, using fluorescently-labelled rhodamine-conjugated phalloidin (ThermoFisher, R415 - described in [45]).

Embryo/oocyte image analysis/ cell counting.

The contribution of each individual cell, per fixed embryo sample (in control or *Kibra/Wwc2* gene RNAi knock-down conditions), to either; inner (entirely encapsulated) outer (whereby a cell retains a cell contactless domain) embryo compartments, emerging blastocyst cell lineages (defined by presence and/or absence of specific and stated lineage marker protein expression), cell populations defined by the presence of a defining intra-cellular feature (*e.g.* cell/nuclei morphological abnormalities, apoptosis or persistent mid-bodies) or presence within or outwith a microinjected clone (distinguishable by a fluorescent injection marker signal, *i.e.* RDBs or recombinant fluorescent fusion proteins) was determined by serial inspection of individual confocal micrograph z-sections of each embryo, using commercial Fluoview ver.1.7.a (Olympus), Imaris (Bitplane) and freely available ImageJ software. These calculated contributions were individually tabulated (see appropriate supplementary tables) and the mean of cells within defined sub-populations, plus standard error of means (mean ± s.e.m.) determined. The statistical significance between relevant experimental and control groups was determined using 2-tailed Student's t-tests (experiment specific supplementary tables provide comprehensive summaries, plus all individual embryo derived data). Relating to oocytes, a similar approach was used to assay the mean frequencies by which maturing oocytes exhibit intra-cellular morphologies (revealed by combined immuno-fluorescent staining, *i.e.* α-TUBULIN and p-AURKA and microinjected fluorescent reporter protein expression *i.e.* RFP-histone H2B) indicative of appropriate or aberrant GV oocyte maturation (as categorised), at the indicated developmental time-point; similarly such data are summarised in relevant supplementary tables, including individual oocyte derived data.

Western blotting

A precise number of oocytes per comparable experimental condition (~15-30) were washed in phosphate buffer saline (PBS; Merck, P5493) containing polyvinyl alcohol (PVA; Merck, 341584), frozen in a residual volume at -80°C, before lysis, in 10 µl of 10x SDS reducing agent/loading buffer (NuPAGE buffer, ThermoFisher Scientific, NP 0004, ThermoFisher Scientific), by boiling at 100°C for 5 minutes. Loaded proteins were electrophoretically separated on gradient precast 4–12% SDS–PAGE gels (ThermoFisher Scientific, NP0323) and transferred to Immobilon P membranes (Merck group, IVPD00010) using a semi-dry blotting system (Biometra/ Analytik Jena) for 25 minutes at 5 mA/ cm^{2}. Blotted membranes were blocked in 5% skimmed milk powder dissolved in 0.05% Tween-Tris pH 7.4 buffered saline (TTBS) for 1 hour, briefly rinsed in TTBS and then incubated overnight at 4°C in 1% milk/TTBS containing primary antibody. Membranes were washed in three changes of TTBS buffer (20 minutes each at room temperature) and horse-radish peroxidase conjugated secondary antibody added to the blot in 1% milk/TTBS, for 1 hour (room temperature). Immuno-detected proteins were visualized by chemiluminescent photographic film exposure (ECL kit; GE Life Sciences, RPN2232) and digitally scanned using a GS-800 calibrated densitometer (Bio-Rad Laboratories). Antibody stripped membrane blots were re-probed, for loading controls, in an identical manner. Supplementary methods tables SM6 details the utilised concentrations of the primary and peroxidase-conjugated secondary antibodies used.

ACKNOWLEDGEMENTS

The authors acknowledge the Animal Facility (Institute of Parasitology, Biology Centre of the Czech Academy of Sciences, České Budějovice, Czech Republic) for housing experimental mice, Marta Gajewska (Institute of Oncology, Warsaw, Poland) and Anna Piliszek (Institute of Genetics & Animal Breeding, Polish Academy of Sciences, Jastrzębiec, Poland) for providing the founder CBA/W mice used in this study, Martin Anger (Central European Institute of Technology (CEITEC)/ Veterinary Research Institute, Brno, Czech Republic) for valuable technical advice and discussions and Alena Krejčí (Faculty of Science, University of South Bohemia, České Budějovice, Czech Republic) for advice and pooling resources. The research was supported by a Czech Science Foundation/ GA ČR grant (18-02891S) awarded to A.W.B. and a Grant Agency of the University of South Bohemia Ph.D. student award to G.V (GA JU: 015/2017/P).

AUTHOR CONTRIBUTION

A.W.B. & G.V. designed the experiments, participated in data analysis (plus A.Š.) and drafted the manuscript (plus A.Š.). G.V. performed all experiments and prepared samples for western blotting (performed by A.Š.). P.B. derived the recombinant DNA constructs and L.G. performed important ancillary experiments, ultimately not included in the final manuscript. A.W.B. coordinated the study. All authors approved the final version of the manuscript for publication.

AUTHOR DECLARATION

The authors declare no competing interests.

726 **REFERENCES**

727

728 1. Johnson MH. From mouse egg to mouse embryo: polarities, axes, and tissues. *Annu Rev Cell*
729 *Dev Biol* **25**, 483-512 (2009).
730

731 2. Sanders JR, Jones KT. Regulation of the meiotic divisions of mammalian oocytes and eggs.
732 *Biochem Soc Trans* **46**, 797-806 (2018).
733

734 3. Hassold T, Hunt P. To err (meiotically) is human: the genesis of human aneuploidy. *Nat Rev*
735 *Genet* **2**, 280-291 (2001).
736

737 4. Nagaoka SI, Hassold TJ, Hunt PA. Human aneuploidy: mechanisms and new insights into an
738 age-old problem. *Nat Rev Genet* **13**, 493-504 (2012).
739

740 5. Bennabi I, Terret ME, Verlhac MH. Meiotic spindle assembly and chromosome segregation in
741 oocytes. *J Cell Biol* **215**, 611-619 (2016).
742

743 6. Namgoong S, Kim NH. Meiotic spindle formation in mammalian oocytes: implications for human
744 infertility. *Biol Reprod* **98**, 153-161 (2018).
745

746 7. Mihajlovic AI, FitzHarris G. Segregating Chromosomes in the Mammalian Oocyte. *Curr Biol* **28**,
747 R895-R907 (2018).
748

749 8. Mogessie B, Scheffler K, Schuh M. Assembly and Positioning of the Oocyte Meiotic Spindle.
750 *Annu Rev Cell Dev Biol* **34**, 381-403 (2018).
751

752 9. Gruss OJ. Animal Female Meiosis: The Challenges of Eliminating Centrosomes. *Cells* **7**, (2018).
753

754 10. Severson AF, von Dassow G, Bowerman B. Oocyte Meiotic Spindle Assembly and Function. *Curr*
755 *Top Dev Biol* **116**, 65-98 (2016).
756

757 11. Courtois A, Schuh M, Ellenberg J, Hiiragi T. The transition from meiotic to mitotic spindle
758 assembly is gradual during early mammalian development. *J Cell Biol* **198**, 357-370 (2012).
759

760 12. Schatten H, Sun QY. The role of centrosomes in mammalian fertilization and its significance for
761 ICSI. *Mol Hum Reprod* **15**, 531-538 (2009).
762

763 13. Sathananthan AH*, et al.* Centrioles in the beginning of human development. *Proc Natl Acad Sci U*
764 *S A* **88**, 4806-4810 (1991).
765

766 14. Li W*, et al.* Differential regulation of H3S10 phosphorylation, mitosis progression and cell fate by
767 Aurora Kinase B and C in mouse preimplantation embryos. *Protein Cell* **8**, 662-674 (2017).
768

769 15. Nguyen AL, Schindler K. Specialize and Divide (Twice): Functions of Three Aurora Kinase
770 Homologs in Mammalian Oocyte Meiotic Maturation. *Trends Genet* **33**, 349-363 (2017).
771

772 16. Saskova A, Solc P, Baran V, Kubelka M, Schultz RM, Motlik J. Aurora kinase A controls meiosis I
773 progression in mouse oocytes. *Cell Cycle* **7**, 2368-2376 (2008).
774

775 17. Nguyen AL*, et al.* Genetic Interactions between the Aurora Kinases Reveal New Requirements
776 for AURKB and AURKC during Oocyte Meiosis. *Curr Biol* **28**, 3458-3468 e3455 (2018).
777

778 18. Solc P*, et al.* Aurora kinase A drives MTOC biogenesis but does not trigger resumption of
779 meiosis in mouse oocytes matured in vivo. *Biol Reprod* **87**, 85 (2012).
780

19. Swain JE, Ding J, Wu J, Smith GD. Regulation of spindle and chromatin dynamics during early and late stages of oocyte maturation by aurora kinases. *Mol Hum Reprod* **14**, 291-299 (2008).

20. Kovarikova V, Burkus J, Rehak P, Brzakova A, Solc P, Baran V. Aurora kinase A is essential for correct chromosome segregation in mouse zygote. *Zygote* **24**, 326-337 (2016).

21. Bury L*, et al.* Plk4 and Aurora A cooperate in the initiation of acentriolar spindle assembly in mammalian oocytes. *J Cell Biol* **216**, 3571-3590 (2017).

22. Coelho PA*, et al.* Spindle formation in the mouse embryo requires Plk4 in the absence of centrioles. *Dev Cell* **27**, 586-597 (2013).

23. Chazaud C, Yamanaka Y. Lineage specification in the mouse preimplantation embryo. *Development* **143**, 1063-1074 (2016).

24. Frum T, Ralston A. Cell signaling and transcription factors regulating cell fate during formation of the mouse blastocyst. *Trends Genet* **31**, 402-410 (2015).

25. Rossant J. Genetic Control of Early Cell Lineages in the Mammalian Embryo. *Annu Rev Genet* **52**, 185-201 (2018).

26. Rossant J. Making the Mouse Blastocyst: Past, Present, and Future. *Curr Top Dev Biol* **117**, 275-288 (2016).

27. White MD, Zenker J, Bissiere S, Plachta N. Instructions for Assembling the Early Mammalian Embryo. *Dev Cell* **45**, 667-679 (2018).

28. Mihajlovic AI, Bruce AW. The first cell-fate decision of mouse preimplantation embryo development: integrating cell position and polarity. *Open Biol* **7**, (2017).

29. O'Farrell PH. Growing an Embryo from a Single Cell: A Hurdle in Animal Life. *Cold Spring Harb Perspect Biol* **7**, (2015).

30. Bolton VN, Oades PJ, Johnson MH. The relationship between cleavage, DNA replication, and gene expression in the mouse 2-cell embryo. *J Embryol Exp Morphol* **79**, 139-163 (1984).

31. Howlett SK, Bolton VN. Sequence and regulation of morphological and molecular events during the first cell cycle of mouse embryogenesis. *J Embryol Exp Morphol* **87**, 175-206 (1985).

32. Krishna M, Generoso WM. Timing of sperm penetration, pronuclear formation, pronuclear DNA synthesis, and first cleavage in naturally ovulated mouse eggs. *J Exp Zool* **202**, 245-252 (1977).

33. Smith RK, Johnson MH. Analysis of the third and fourth cell cycles of mouse early development. *J Reprod Fertil* **76**, 393-399 (1986).

34. Parisi E, Filosa S, De Petrocellis B, Monroy A. The pattern of cell division in the early development of the sea urchin. Paracentrotus lividus. *Dev Biol* **65**, 38-49 (1978).

35. Newport J, Kirschner M. A major developmental transition in early Xenopus embryos: I. characterization and timing of cellular changes at the midblastula stage. *Cell* **30**, 675-686 (1982).

36. Foe VE, Alberts BM. Studies of nuclear and cytoplasmic behaviour during the five mitotic cycles that precede gastrulation in Drosophila embryogenesis. *J Cell Sci* **61**, 31-70 (1983).

37. O'Farrell PH, Stumpff J, Su TT. Embryonic cleavage cycles: how is a mouse like a fly? *Curr Biol* **14**, R35-45 (2004).

837
838 38. Davis JR, Tapon N. Hippo signalling during development. *Development* **146**, (2019).
839
840 39. Leung CY, Zernicka-Goetz M. Angiomotin prevents pluripotent lineage differentiation in mouse
841 embryos via Hippo pathway-dependent and -independent mechanisms. *Nat Commun* **4**, 2251
842 (2013).
843
844 40. Nishioka N*, et al.* The Hippo signaling pathway components Lats and Yap pattern Tead4 activity
845 to distinguish mouse trophectoderm from inner cell mass. *Dev Cell* **16**, 398-410 (2009).
846
847 41. Cockburn K, Biechele S, Garner J, Rossant J. The Hippo pathway member Nf2 is required for
848 inner cell mass specification. *Curr Biol* **23**, 1195-1201 (2013).
849
850 42. Kono K, Tamashiro DA, Alarcon VB. Inhibition of RHO-ROCK signaling enhances ICM and
851 suppresses TE characteristics through activation of Hippo signaling in the mouse blastocyst. *Dev*
852 *Biol* **394**, 142-155 (2014).
853
854 43. Alarcon VB. Cell polarity regulator PARD6B is essential for trophectoderm formation in the
855 preimplantation mouse embryo. *Biol Reprod* **83**, 347-358 (2010).
856
857 44. Hirate Y*, et al.* Polarity-dependent distribution of angiomotin localizes Hippo signaling in
858 preimplantation embryos. *Curr Biol* **23**, 1181-1194 (2013).
859
860 45. Mihajlovic AI, Bruce AW. Rho-associated protein kinase regulates subcellular localisation of
861 Angiomotin and Hippo-signalling during preimplantation mouse embryo development. *Reprod*
862 *Biomed Online* **33**, 381-390 (2016).
863
864 46. Nishioka N*, et al.* Tead4 is required for specification of trophectoderm in pre-implantation mouse
865 embryos. *Mechanisms of development* **125**, 270-283 (2008).
866
867 47. Yagi R*, et al.* Transcription factor TEAD4 specifies the trophectoderm lineage at the beginning of
868 mammalian development. *Development* **134**, 3827-3836 (2007).
869
870 48. Mihajlovic AI, Thamodaran V, Bruce AW. The first two cell-fate decisions of preimplantation
871 mouse embryo development are not functionally independent. *Sci Rep* **5**, 15034 (2015).
872
873 49. Sasaki H. Roles and regulations of Hippo signaling during preimplantation mouse development.
874 *Dev Growth Differ* **59**, 12-20 (2017).
875
876 50. Hirate Y, Hirahara S, Inoue K, Kiyonari H, Niwa H, Sasaki H. Par-aPKC-dependent and -
877 independent mechanisms cooperatively control cell polarity, Hippo signaling, and cell positioning
878 in 16-cell stage mouse embryos. *Dev Growth Differ* **57**, 544-556 (2015).
879
880 51. Wicklow E*, et al.* HIPPO pathway members restrict SOX2 to the inner cell mass where it
881 promotes ICM fates in the mouse blastocyst. *PLoS Genet* **10**, e1004618 (2014).
882
883 52. Frum T, Murphy TM, Ralston A. HIPPO signaling resolves embryonic cell fate conflicts during
884 establishment of pluripotency in vivo. *Elife* **7**, (2018).
885
886 53. Frum T, Watts JL, Ralston A. TEAD4, YAP1 and WWTR1 prevent the premature onset of
887 pluripotency prior to the 16-cell stage. *Development* **146**, (2019).
888
889 54. Hashimoto M, Sasaki H. Epiblast Formation by TEAD-YAP-Dependent Expression of
890 Pluripotency Factors and Competitive Elimination of Unspecified Cells. *Dev Cell* **50**, 139-154
891 e135 (2019).
892

55. Kremerskothen J, *et al.* Characterization of KIBRA, a novel WW domain-containing protein. *Biochem Biophys Res Commun* **300**, 862-867 (2003).

56. Genevet A, Wehr MC, Brain R, Thompson BJ, Tapon N. Kibra is a regulator of the Salvador/Warts/Hippo signaling network. *Dev Cell* **18**, 300-308 (2010).

57. Baumgartner R, Poernbacher I, Buser N, Hafen E, Stocker H. The WW domain protein Kibra acts upstream of Hippo in Drosophila. *Dev Cell* **18**, 309-316 (2010).

58. Yu J, Zheng Y, Dong J, Klusza S, Deng WM, Pan D. Kibra functions as a tumor suppressor protein that regulates Hippo signaling in conjunction with Merlin and Expanded. *Dev Cell* **18**, 288-299 (2010).

59. Xiao L, Chen Y, Ji M, Dong J. KIBRA regulates Hippo signaling activity via interactions with large tumor suppressor kinases. *J Biol Chem* **286**, 7788-7796 (2011).

60. Wennmann DO, *et al.* Evolutionary and molecular facts link the WWC protein family to Hippo signaling. *Mol Biol Evol* **31**, 1710-1723 (2014).

61. Lin Z, Yang Z, Xie R, Ji Z, Guan K, Zhang M. Decoding WW domain tandem-mediated target recognitions in tissue growth and cell polarity. *Elife* **8**, (2019).

62. Wang W, Li X, Huang J, Feng L, Dolinta KG, Chen J. Defining the protein-protein interaction network of the human hippo pathway. *Mol Cell Proteomics* **13**, 119-131 (2014).

63. Zhang Y, *et al.* WWC2 is an independent prognostic factor and prevents invasion via Hippo signalling in hepatocellular carcinoma. *J Cell Mol Med* **21**, 3718-3729 (2017).

64. Han Q, *et al.* WWC3 inhibits epithelial-mesenchymal transition of lung cancer by activating Hippo-YAP signaling. *Onco Targets Ther* **11**, 2581-2591 (2018).

65. Zenker J, *et al.* A microtubule-organizing center directing intracellular transport in the early mouse embryo. *Science* **357**, 925-928 (2017).

66. Johnson MH, Ziomek CA. The foundation of two distinct cell lineages within the mouse morula. *Cell* **24**, 71-80 (1981).

67. Strumpf D, *et al.* Cdx2 is required for correct cell fate specification and differentiation of trophectoderm in the mouse blastocyst. *Development* **132**, 2093-2102 (2005).

68. Terada Y, Tatsuka M, Suzuki F, Yasuda Y, Fujita S, Otsu M. AIM-1: a mammalian midbody-associated protein required for cytokinesis. *EMBO J* **17**, 667-676 (1998).

69. Salles FJ, Darrow AL, O'Connell ML, Strickland S. Isolation of novel murine maternal mRNAs regulated by cytoplasmic polyadenylation. *Genes Dev* **6**, 1202-1212 (1992).

70. Koncicka M, *et al.* Increased Expression of Maturation Promoting Factor Components Speeds Up Meiosis in Oocytes from Aged Females. *Int J Mol Sci* **19**, (2018).

71. Makuch L, *et al.* Regulation of AMPA receptor function by the human memory-associated gene KIBRA. *Neuron* **71**, 1022-1029 (2011).

72. Xiao L, *et al.* KIBRA protein phosphorylation is regulated by mitotic kinase aurora and protein phosphatase 1. *J Biol Chem* **286**, 36304-36315 (2011).

73. Zhang L*, et al.* KIBRA regulates aurora kinase activity and is required for precise chromosome alignment during mitosis. *J Biol Chem* **287**, 34069-34077 (2012).

74. Yabuta N*, et al.* Lats2 is an essential mitotic regulator required for the coordination of cell division. *J Biol Chem* **282**, 19259-19271 (2007).

75. Abe Y, Ohsugi M, Haraguchi K, Fujimoto J, Yamamoto T. LATS2-Ajuba complex regulates gamma-tubulin recruitment to centrosomes and spindle organization during mitosis. *FEBS Lett* **580**, 782-788 (2006).

76. Asteriti IA, De Mattia F, Guarguaglini G. Cross-Talk between AURKA and Plk1 in Mitotic Entry and Spindle Assembly. *Front Oncol* **5**, 283 (2015).

77. Lu LY*, et al.* Polo-like kinase 1 is essential for early embryonic development and tumor suppression. *Mol Cell Biol* **28**, 6870-6876 (2008).

78. Habedanck R, Stierhof YD, Wilkinson CJ, Nigg EA. The Polo kinase Plk4 functions in centriole duplication. *Nat Cell Biol* **7**, 1140-1146 (2005).

79. Bettencourt-Dias M*, et al.* SAK/PLK4 is required for centriole duplication and flagella development. *Curr Biol* **15**, 2199-2207 (2005).

80. Zernicka-Goetz M*, et al.* An indelible lineage marker for Xenopus using a mutated green fluorescent protein. *Development* **122**, 3719-3724 (1996).

81. Horn T, Boutros M. E-RNAi: a web application for the multi-species design of RNAi reagents--2010 update. *Nucleic Acids Res* **38**, W332-339 (2010).

82. Morris SA, Teo RT, Li H, Robson P, Glover DM, Zernicka-Goetz M. Origin and formation of the first two distinct cell types of the inner cell mass in the mouse embryo. *Proc Natl Acad Sci U S A* **107**, 6364-6369 (2010).

83. Lemaire P, Garrett N, Gurdon JB. Expression cloning of Siamois, a Xenopus homeobox gene expressed in dorsal-vegetal cells of blastulae and able to induce a complete secondary axis. *Cell* **81**, 85-94 (1995).

84. Livak KJ, Schmittgen TD. Analysis of relative gene expression data using real-time quantitative PCR and the 2(-Delta Delta C(T)) Method. *Methods (San Diego, Calif* **25**, 402-408 (2001).

FIGURE LEGENDS

Figure 1: dsRNA mediated WWC-domain containing gene (*Kibra* and *Wwc2*) expression knockdown in preimplantation stage mouse embryos is associated with (*Wwc2*) reduced cell number. a) Experimental schema of *Kibra* and *Wwc2* specific dsRNA (plus *EGFP n*egative control) embryo microinjection mediated global mRNA knockdown, followed by *in vitro* culture to either 8-cell (E2.5) or 32-cell (E3.5) stage and Q-RT-PCR analysis (upper). Normalised mRNA expression of either *Kibra* or *Wwc2* derived mRNAs after microinjection of stated dsRNA at the stated developmental stage (lower; error bars represent s.e.m. and n=3). **b)** Experimental schema, similar to a), describing clonal *Kibra*, *Wwc2* or *Kibra+Wwc2* knockdown (microinjection of one cell at the 2-cell/E1.5 stage) and total cell number assay (via fixed embryo DAPI staining) at the late blastocyst, >64-cell (E4.5) stage (upper). Average total cell numbers per embryo in each stated dsRNA microinjection group is shown (lower chart). **c)** Experimental strategy to knockdown *Wwc2* expression (as in b) in a marked clone, by co-microinjection of *Wwc2* dsRNA with rhodamine conjugated dextran microbeads (RDBs; fluorescent lineage marker) and assay clonal contribution at the 16-cell (E3.0) stage (upper). Average total cell number per clone (*i.e.* 'Inj'. vs. 'Non') in *Wwc2* or control dsRNA microinjection groups are shown, as determined by the relative position of individual cells within the embryo (*i.e.* encapsulated inside or with a cell contactless domain on the outside; lower chart). In panels b) & c) chart error bars represent s.e.m. and 'n' numbers are indicated; statistically significant differences (2-tailed students t-test) between the experimental microinjection groups (asterisks), or clones ('Inj.' vs. 'Non') within a group (double crosses), are highlighted with statistical confidence intervals of $p<0.05$ and $p<0.005$, as denoted by one or two significance markers, respectively; in panel b) a lack of significant difference between the compared groups is marked 'n.s.'. Supplementary tables ST1 and ST2 summarise the statistical analysis and individual embryo data.

Figure 2: siRNA mediated global *Wwc2* knockdown causes persistent preimplantation stage cell number deficits from the 8-cell stage onwards: a) Experimental design; non-specific control or *Wwc2*-specific siRNA were co-microinjected with RDBs, into both blastomeres at the 2-cell (E1.5) stage, and *in vitro* cultured, fixed and subject to total cell assay count (via DAPI and phalloidin staining) at the indicated developmental stage. A separate group of microinjected embryos at the 32-cell stage were subject to normalised *Wwc2*-specific Q-RTPCR to assay knockdown efficiency. **b)** Q-RTPCR data detailing the extent of endogenous *Wwc2* expression knockdown caused by microinjected *Wwc2*-specific siRNA at the 32-cell (E3.5) stage (error bars denote s.e.m. of triplicate measurements, n=3). **c)** Average total cell number in control (blue bars) or *Wwc2*-specific (green bars) siRNA microinjected embryos at each indicated preimplantation developmental stages (the number of embryos in each assayed group is indicated). Errors represent s.e.m. and 2-tailed student t-test derived statistical significance between the control and *Wwc2* knockdown groups, at defined developmental stages, indicated (** $p<0.005$). Supplementary tables ST3-ST8 summarise the statistical analysis and individual embryo data in each experimental group. Note, additional data describing the frequency of observable cell morphological/ division defects, obtained from this exact same dataset are presented in Fig. 3.

Figure 3: Global *Wwc2* knockdown mediated cell numbers deficits are coincident with accumulated cell morphologies consistent with defective cell division. a) Schematic of experimental design whereby 2-cell (E1.5)

stage embryos microinjected with either control or *Wwc2*-specific siRNA were *in vitro* cultured to the indicated developmental stage, fixed and assayed for total cell number (as described in Fig. 2) and the incidence of abnormal cell/embryo morphology indicative of aberrant cell division, as determined by DAPI and rhodamine conjugated phalloidin staining (note, data described in this figure are derived from same experiments as those described in Fig. 2). **b)** Exemplar confocal micrograph z-sections of *Wwc2*-specific siRNA microinjected embryos at the 32-cell (E3.5) stage, illustrating three distinct categories of observed phenotypic morphological defects; i. abnormal nuclear morphology (including chromatin mid body association - left), ii. cytokinesis defects defined by presence of two nuclei per cell (centre), iii. presence of multiple (*i.e.* >2) nuclei and/or micronuclei per cell (right) and iv. a composite of categorised defects highlighted by colour coded arrows in single embryo confocal z-section projection (green boarder). DAPI (white) and cortical F-actin (red); scale bar = 20 μm. **c)** Frequencies of each the observed categories of phenotypic/ morphological defect (*i.e.* micronuclei; blue, abnormal nuclei; yellow and failed cytokinesis; green) or a combination of at least two or more (red) in control siRNA (left) and *Wwc2*-specific siRNA (right) microinjected embryos, at the indicated developmental stage (numbers of embryos in each group is highlighted); data demonstrate defect incidence per embryo (in at least one constituent blastomere – upper row of charts) or on a per cell assayed basis (lower row of charts). Supplementary tables ST3-ST8 summarise the statistical analysis and individual embryo data in each experimental group.

Figure 4: Outer trophectoderm (TE) versus ICM derivation in clonal *Wwc2* gene knockdown at the early blastocyst stage. a) Experimental strategy for *Wwc2* expression knockdown in a marked clone (representing 50% of the embryo) by co-microinjection (in one blastomere of 2-cell/E1.5 stage embryos) of *Wwc2* siRNA and GAP43-GFP mRNA (stable plasma membrane fluorescent lineage marker – 'Inj.') and an immunofluorescence (IF) based assay of clonal contribution ('Inj' vs. 'Non') to CDX2 (TE marker) positive or negative cells, plus outer and inner-cell embryo populations, at 32-cell (E3.5) stage (versus similar control siRNA microinjections). **b)** Exemplar confocal z-section micrographs of IF stained blastocysts (individual greyscale channels plus merged image; CDX2 is red) from control and *Wwc2* siRNA microinjected groups. Note, white arrows and the yellow arrow head denote DAPI stained micronuclei and a bi-nucleated cell uniquely found within the *Wwc2* siRNA microinjected clone, respectively. Similarly, blue and white asterisks denote respective low level (compared to non-injected clone) or undetectable outer-cell CDX2 protein expression in *Wwc2* knockdown clones. The number of embryos in each group is provided; scale bar equals 20μm. **c)** Left - pie charts detailing the average distribution of detectable CDX2 protein expression between the control and *Wwc2* siRNA groups, in both outer or ICM cells (note, pie chart areas for each spatial population are scaled to that summarising the whole embryo; similarly, the pie chart area describing the whole embryo in the *Wwc2* siRNA condition is scaled to that in the control siRNA group). Right - average clonal contribution ('Inj' vs. 'Non') of outer and ICM cells in control (blue bars) and *Wwc2* siRNA (green bars) microinjected embryos, irrespective of CDX2 expression. **d)** As in c) only describing the clonal contribution of CDX2 expressing (or not) cells to outer and ICM populations, as a fraction of the total sub-population size (left - pie charts) or in raw average cell number (right – bar charts) In panel c) and d) charts, errors represent s.e.m. and 2-tailed student t-test derived statistical significance between the control and *Wwc2* knockdown groups (asterisks), or clones ('Inj.' vs 'Non') within a group (double crosses), are highlighted with statistical confidence intervals of $p<0.05$ and $p<0.005$, as denoted by

one or two significance markers, respectively. Supplementary tables ST14 summarise the statistical analysis and individual embryo data.

Figure 5: Overall cell lineage derivation in clonal *Wwc2* gene knockdown at the late blastocyst stage. a) Experimental strategy for *Wwc2* expression knockdown in a marked clone (representing 50% of the embryo) by co-microinjection (in one blastomere of 2-cell/E1.5 stage embryos) of *Wwc2* siRNA and GAP43-GFP mRNA (stable plasma membrane fluorescent lineage marker – 'Inj.') and an IF based assay of clonal contribution ('Inj' vs. 'Non') to blastocyst protein lineage marker (TE; CDX2, PrE; GATA4, EPI; NANOG or SOX2; assayed in combination – see below) expressing cells, plus outer and inner-cell embryo populations, at >64-cell, late blastocyst (E4.5) stage (versus similar control siRNA microinjections). **b)** Average number of apoptotic cells observed in control and *Wwc2* siRNA microinjected embryo groups (averaged across all IF regimes – see below) between outer and inner cell populations and clones ('Inj.' vs. 'Non'); errors represent s.e.m. and 2-tailed student t-test derived statistical significance between the control and *Wwc2* knockdown groups (asterisks), or clones ('Inj.' vs 'Non') within a group (double crosses), are highlighted with statistical confidence intervals of $p<0.05$ and $p<0.005$, as denoted by one or two significance markers, respectively. **c)** Exemplar confocal z-section micrographs of IF stained blastocysts (individual greyscale channels plus merged image, in which assayed combinations of cell lineage markers are respectively coloured green and red; CDX2 & NANOG, GATA4 & NANOG and GATA4 and SOX2) from control and *Wwc2* siRNA microinjected groups. Within the *Wwc2* siRNA microinjected clone, yellow arrows denote apoptotic cell remnants, blue arrows interphase ICM cells that neither express GATA4 or NANOG, the yellow arrow head a bi-nucleated cell whereas blue or white asterisks highlight outer-cells with basal or undetectable CDX2 expression, respectively. The number of assayed embryos in each control ('Con') and *Wwc2* siRNA ('KD') microinjection group is provided; scale bar equals 20µm. **d)** Pie charts detailing, in the left panel, the average distribution of detectable CDX2 and NANOG protein expression between the control and *Wwc2* siRNA groups, in both outer or ICM cells (note, pie chart areas for each spatial population are scaled to that summarising the whole embryo; similarly the pie chart area describing the whole embryo in the *Wwc2* siRNA condition is scaled to that in the control siRNA group). Central and right panels contain pie charts describing the clonal contribution of CDX2 and NANOG expressing (or not) cells to outer and ICM populations, as a fraction of the total sub-population size. **e)** As in d) only assaying NANOG (EPI) and GATA4 (PrE) expression. **f)** As in d) only assaying SOX2 (EPI) and GATA4 (PrE) expression. Note, supplementary figure S4 details the same data in raw average cell number format (*i.e.* as presented in Fig. 4, panel d) - bar charts on right) and supplementary tables ST15-ST17 summarise the statistical analysis and individual embryo data.

Figure 6: Expression of siRNA resistant recombinant *HA-Wwc2* mRNA rescues *Wwc2* siRNA elicited cell number/ division phenotypes. a) Experimental strategy to assay potential phenotypic rescue of clonal *Wwc2* expression knockdown by comparing co-microinjection (in one blastomere of 2-cell/E1.5 stage embryos) of GAP43-GFP mRNA (stable plasma membrane fluorescent lineage marker – 'Inj.') with either control siRNA, *Wwc2* siRNA or *Wwc2* siRNA + recombinant *HA-Wwc2* mRNA (containing a N-terminal HA-epitope tag and point mutations conferring siRNA resistance – see supplementary figure S5) and assaying total, outer and inner-cell number at the 32- (E3.5) and >64-cell (late blastocyst/E4.5) stages. **b)** Average clonal contribution ('Inj' vs. 'Non') of outer and

ICM cells in control siRNA (blue bars), *Wwc2* siRNA (green bars) and *Wwc2* siRNA + *HA-Wwc2* mRNA (rescue – orange bars) microinjected embryos; errors represent s.e.m. and 2-tailed student t-test derived statistical significance between the three experimental groups (asterisks), or clones ('Inj.' vs 'Non') within a group (double crosses), are highlighted with statistical confidence intervals of $p<0.05$ and $p<0.005$, as denoted by one or two significance markers, respectively. The number of embryos in each experimental group is provided. **c)** Pie charts detailing the overall and clonal distribution of constituent embryo cells between outer and inner-cell populations, plus the incidence of abnormal nuclear morphology (as defined in Fig. 3), in each of the three indicated experimental groups, at the 32-cell/E3.5 early blastocyst (left) and >64-cell/E4.5 late blastocyst (right) stages. Note, the areas of all individual pie chart categories are normalised against those describing the appropriate criteria in the control siRNA condition. **d)** Exemplar confocal z-section micrographs of 32-cell/E3.5 early and >64-cell/E4.5 late blastocysts of the indicated microinjection groups IF stained to detect HA-epitope tag expression (individual greyscale channels plus merged images, in which the anti-HA channel is coloured red and the DAPI cyan). Within the microinjected clone of the *Wwc2* siRNA treated group, white or red asterisks respectively denote characteristic abnormal mitotic or apoptotic cell remnants, whilst in the microinjected clone of the *Wwc2* siRNA + *HA-Wwc2* rescue group, white arrows indicate anti-HA epitope tag signal associated with cell junctions, particular characteristic, in 32-cell (E3.5) stage embryos, as mid-bodies (see also indicated zoomed images); scale bar equals 20μm. Supplementary tables ST18 & ST19 summarise the statistical analysis and individual embryo data used to generate the figure.

Figure 7: *Wwc2* mRNA is required for mouse oocyte meiotic maturation. a) Published microarray (Wang et al., 2004, blue line) and generated Q-RT-PCR (bar charts) normalised *Wwc2* mRNA expression in germinal vesicle and metaphase II arrested oocytes (GV and MII) and fertilised zygotes (*Tbp* normalised expression, relative to GV stage expression). Note, microarray data derived from oligo-dT primed reverse transcription and Q-RT-PCR from both oligo-dT (black bars) and random hexamer priming (red bars); error bars represent s.e.m. and n=3. **b)** Taken from our published mRNA-Seq dataset of polysome-associated (red) and non-associated (blue) transcripts in *in vitro* maturing mouse oocytes (after germinal vesicle breakdown/ GVBD +3 hours) (Koncicka *et al.,* 2018). **c)** Experimental schema of *Wwc2* transcript knockdown in GV oocytes by microinjected *Wwc2* siRNA (plus control siRNA and non-microinjected controls), 18 hour incubation in IMBX containing media (to prevent GVBD), 16 hour *in vitro* oocyte maturation (IVM – minus IMBX treatment) and confocal microscopy/ Q-RT-PCR analysis; co-microinjected RDBs were used as injection control marker. **d)** Q-RT-PCR data of normalised (against *Tbp* transcripts) *Wwc2* mRNA levels in control and *Wwc2* siRNA microinjected GV oocytes matured to the MII stage; expressed as percentage *Wwc2* mRNA knockdown, versus control (left), and normalised expression levels (right - error bars represent s.e.m. and n=3). **e)** Charts (left) detailing successful maturation frequencies of control non-microinjected (Non-Inj), microinjected control siRNA (Con. siRNA) and microinjected *Wwc2* siRNA GV oocytes, to the MII stage or preceding phenotypic stages. Examples of successfully matured MII oocytes (note, extruded first polar body/PB1) and the quantified categorised phenotypes are shown as confocal z-section micrographs (right – α-Tubulin in green and DAPI DNA pseudo-coloured red; scale bar = 20 μm). Supplementary tables ST21 summarise the statistical analysis and individual oocyte data used to generate the figure.

155 **Figure 8: *Wwc2* knockdown induced GV oocyte IVM phenotypes are associated with failed Aurora-A**
156 **(AURKA) phosphorylation/activation; both rescuable by co-microinjection of siRNA resistant *HA-Wwc2***
157 **mRNA. a)** Experimental schema of GV oocyte microinjection conditions; *i.e. Wwc2* siRNA or control siRNA alone
158 or *Wwc2* siRNA + *HA-Wwc2* (siRNA resistant) mRNA, each co-microinjected with either RDBs (for western blot
159 analysis) or RFP-H2B mRNA (IF – fluorescent marker). Microinjected (plus non-microinjected control) GV oocytes
160 were incubated in IMBX containing media (18 hours - to prevent GVBD), subject to IVM (max. 16 hours – media
161 minus IMBX) and processed for western blotting and IF at designated oocyte maturation time-points (assaying
162 phospho-Aurora/ p-AURKA levels: p-Thr288) or assayed for developmental progression/*Wwc2* knockdown induced
163 IVM phenotypes. **b)** Western blots of activated p-AURKA levels (plus GAPDH housekeeping control), at indicated
164 stages of oocyte maturation (note, GV; +0 hours relative to IMBX washout, metaphase of meiosis I/ MI; +7 hours
165 and MII; +16 hours), in either control or *Wwc2* siRNA microinjected, or non-microinjected conditions. **c)** Exemplar
166 single confocal z-section IF micrographs of control (left) or *Wwc2* siRNA (right) IVM cultured microinjected oocytes
167 to the MII stage (relative to control; 16 hours post-IBMX) stained for p-AURKA (green) and α-TUBULIN (white)
168 and labelled with RFP-H2B chromatin reporter (red); insets show zoomed region of meiotic spindle. *Wwc2* siRNA
169 microinjection group example image is over-saturated compared to control (illustrating lack of spindle associated
170 pAURKA); PB1 (control siRNA) denotes the extruded first polar body and the scale bars represents 20 μm. **d)** Charts
171 detailing the maturation of control siRNA, *Wwc2* siRNA and *Wwc2* siRNA + *HA-Wwc2* mRNA microinjected GV
172 oocytes at staged time-points after IBMX removal; as described by the percentage of oocytes at any of the stated
173 IVM stages or categorised phenotypes (typically associated with *Wwc2* knockdown – see Fig. 7). **e)** Western blot of
174 activated p-AURKA levels (plus GAPDH housekeeping control), at the MII equivalent stage (16 hours post-IVM),
175 in either control siRNA, *Wwc2* siRNA or *Wwc2* siRNA + *HA-Wwc2* mRNA initially microinjected GV oocytes.
176 Supplementary tables ST23-26 summarise the statistical analysis and individual oocyte data used to generate the
177 figure.
178

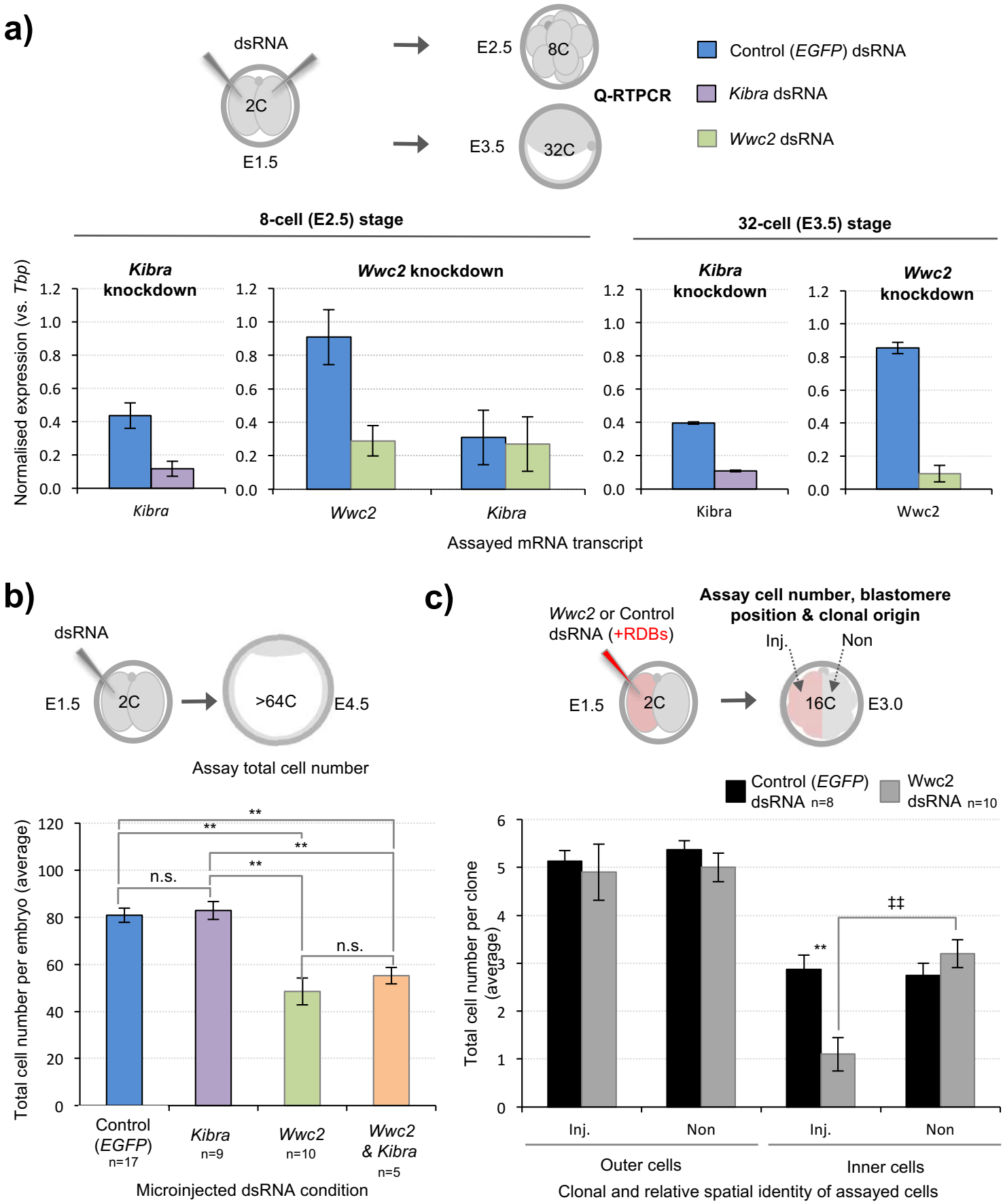
a)
dsRNA
2C
E1.5
E2.5
8C
E3.5
32C
Q-RTPCR
Control (EGFP) dsRNA
Kibra dsRNA
Wwc2 dsRNA
8-cell (E2.5) stage
32-cell (E3.5) stage
Kibra knockdown
Wwc2 knockdown
Kibra knockdown
Wwc2 knockdown
Normalised expression (vs. Tbp)
1.2
1.0
0.8
0.6
0.4
0.2
0.0
Kibra
Wwc2
Kibra
Kibra
Wwc2
Assayed mRNA transcript
b)
dsRNA
E1.5
2C
>64C
E4.5
Assay total cell number
Total cell number per embryo (average)
120
100
80
60
40
20
0
**
**
**
**
n.s.
n.s.
Control (EGFP) n=17
Kibra n=9
Wwc2 n=10
Wwc2 & Kibra n=5
Microinjected dsRNA condition
c)
Wwc2 or Control dsRNA (+RDBs)
Assay cell number, blastomere position & clonal origin
Inj.
Non
E1.5
2C
16C
E3.0
Control (EGFP) dsRNA n=8
Wwc2 dsRNA n=10
Total cell number per clone (average)
6
5
4
3
2
1
0
**
‡‡
Inj.
Non
Inj.
Non
Outer cells
Inner cells
Clonal and relative spatial identity of assayed cells

Fig. 1

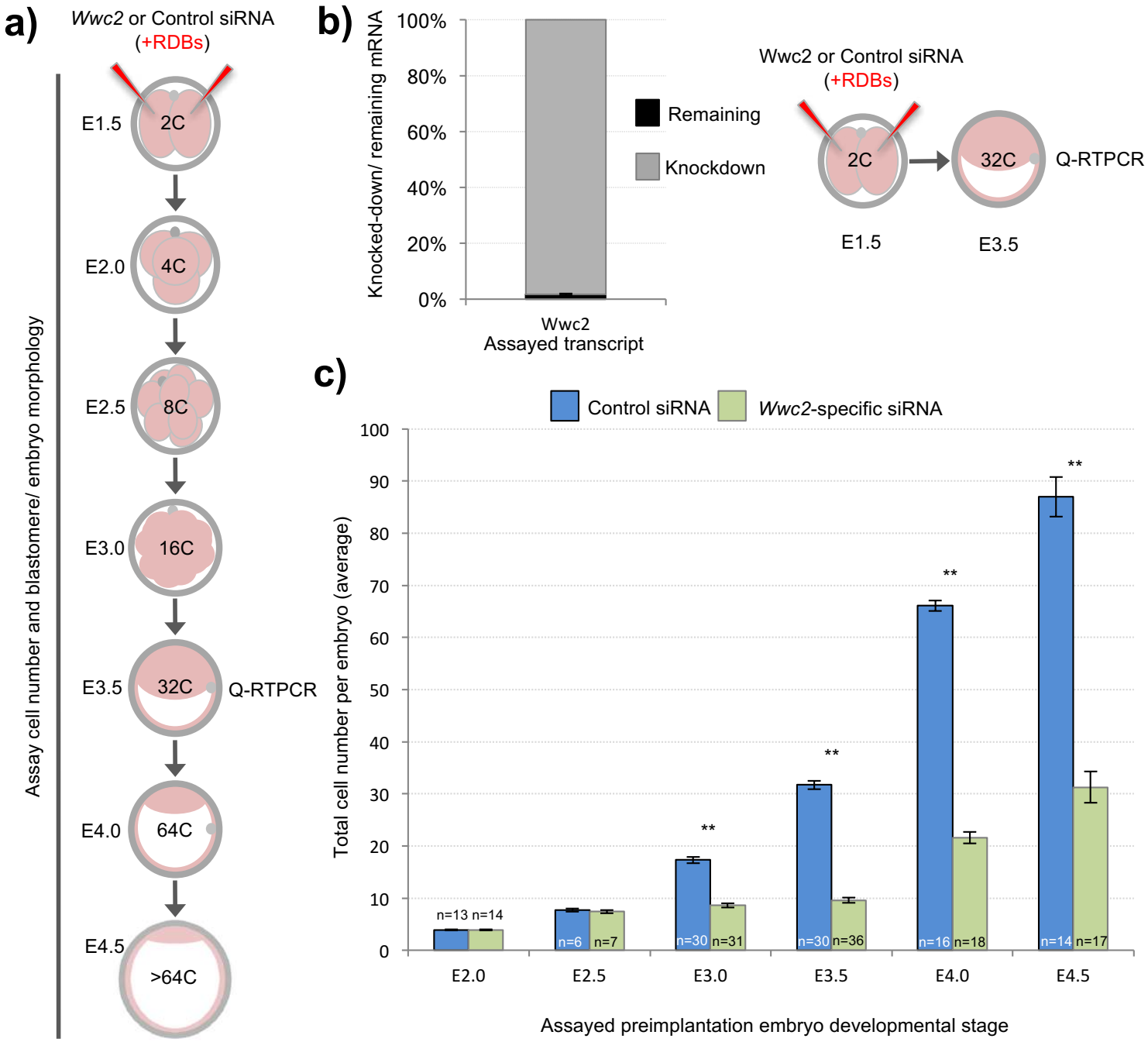
a)
Wwc2 or Control siRNA
(+RDBs)
E1.5
2C
E2.0
4C
E2.5
8C
E3.0
16C
E3.5
32C
Q-RTPCR
E4.0
64C
E4.5
>64C
Assay cell number and blastomere/ embryo morphology
b)
Knocked-down/ remaining mRNA
100%
80%
60%
40%
20%
0%
Remaining
Knockdown
Wwc2
Assayed transcript
Wwc2 or Control siRNA
(+RDBs)
2C
32C
Q-RTPCR
E1.5
E3.5
c)
Control siRNA
Wwc2-specific siRNA
Total cell number per embryo (average)
100
90
80
70
60
50
40
30
20
10
0
**
n=13 n=14
n=6
n=7
n=30
n=31
n=30
n=36
n=16
n=18
n=14
n=17
E2.0
E2.5
E3.0
E3.5
E4.0
E4.5
Assayed preimplantation embryo developmental stage

Fig. 2

Fig. 3

a)

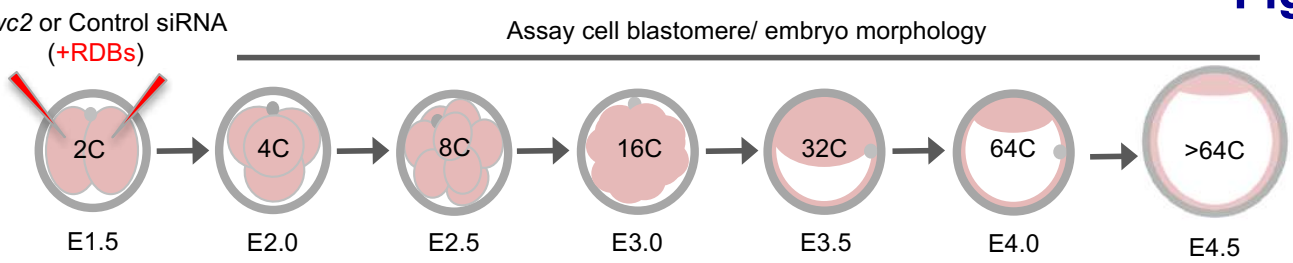

b)

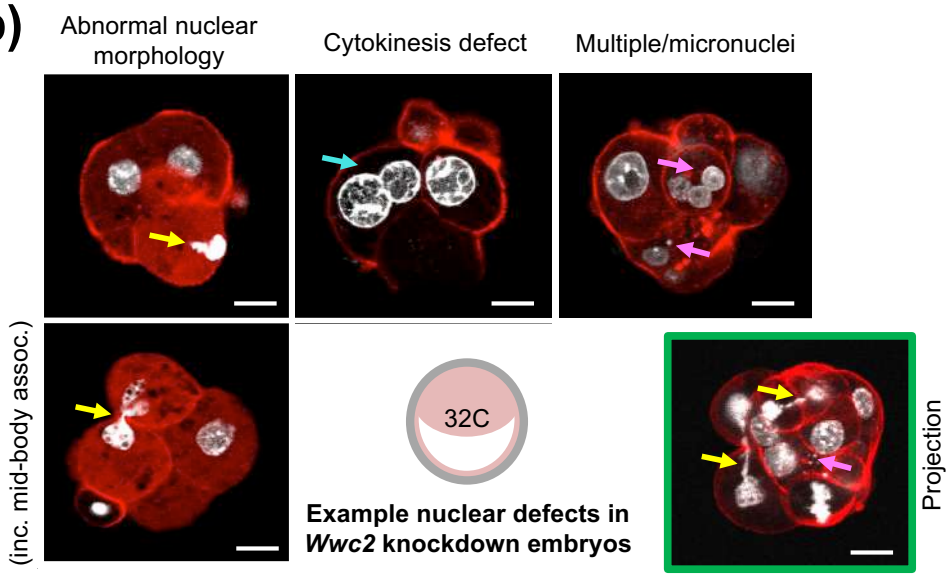

c)

Phenotype		
Presence of multiple/ micronuclei	Observed	
	Unobserved	
Abnormal nuclear morphology	Observed	
	Unobserved	
Cytokinesis defect	Observed	
	Unobserved	
Amalgamated phenotypes	Observed	
	Unobserved	

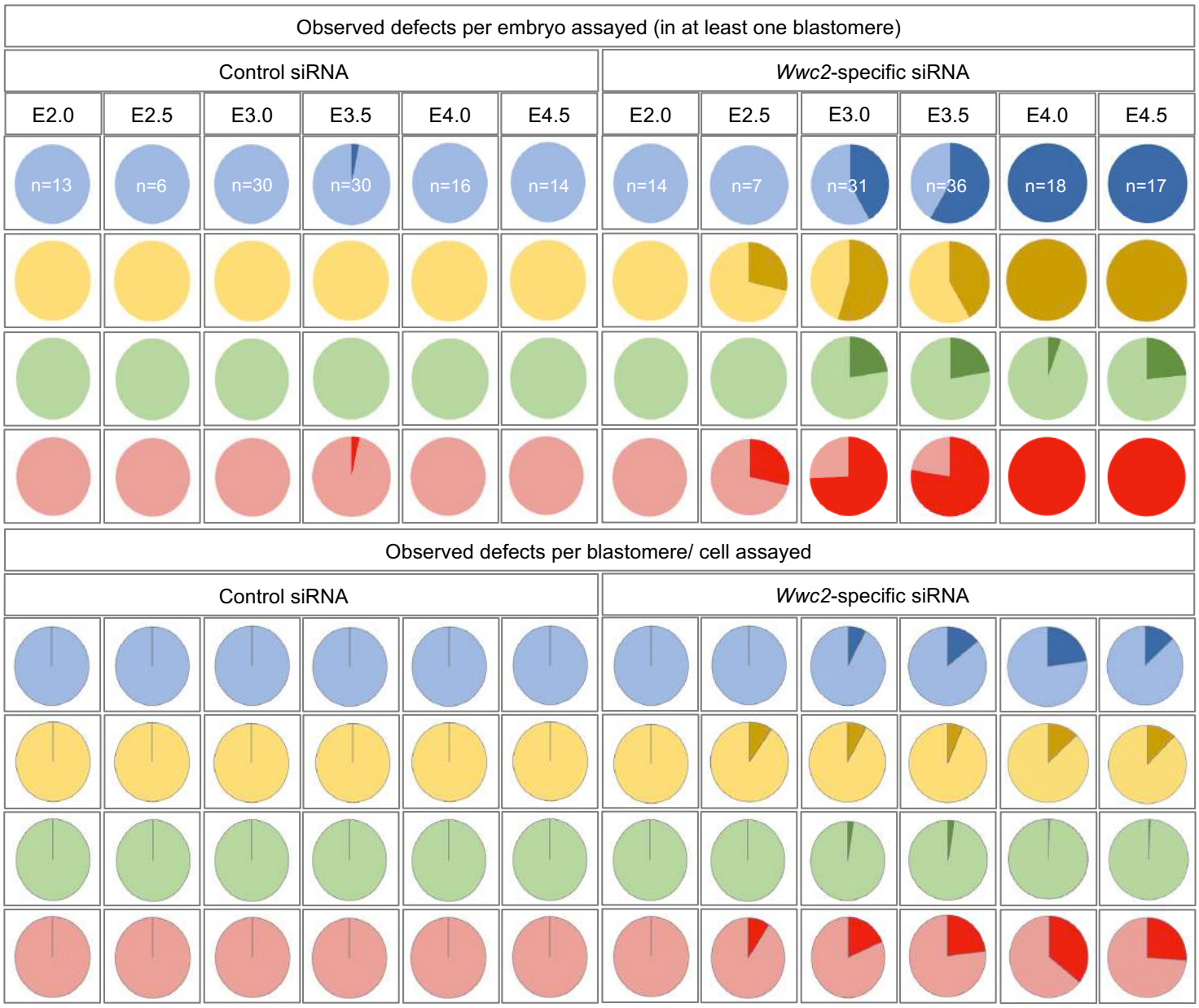

Fig. 4

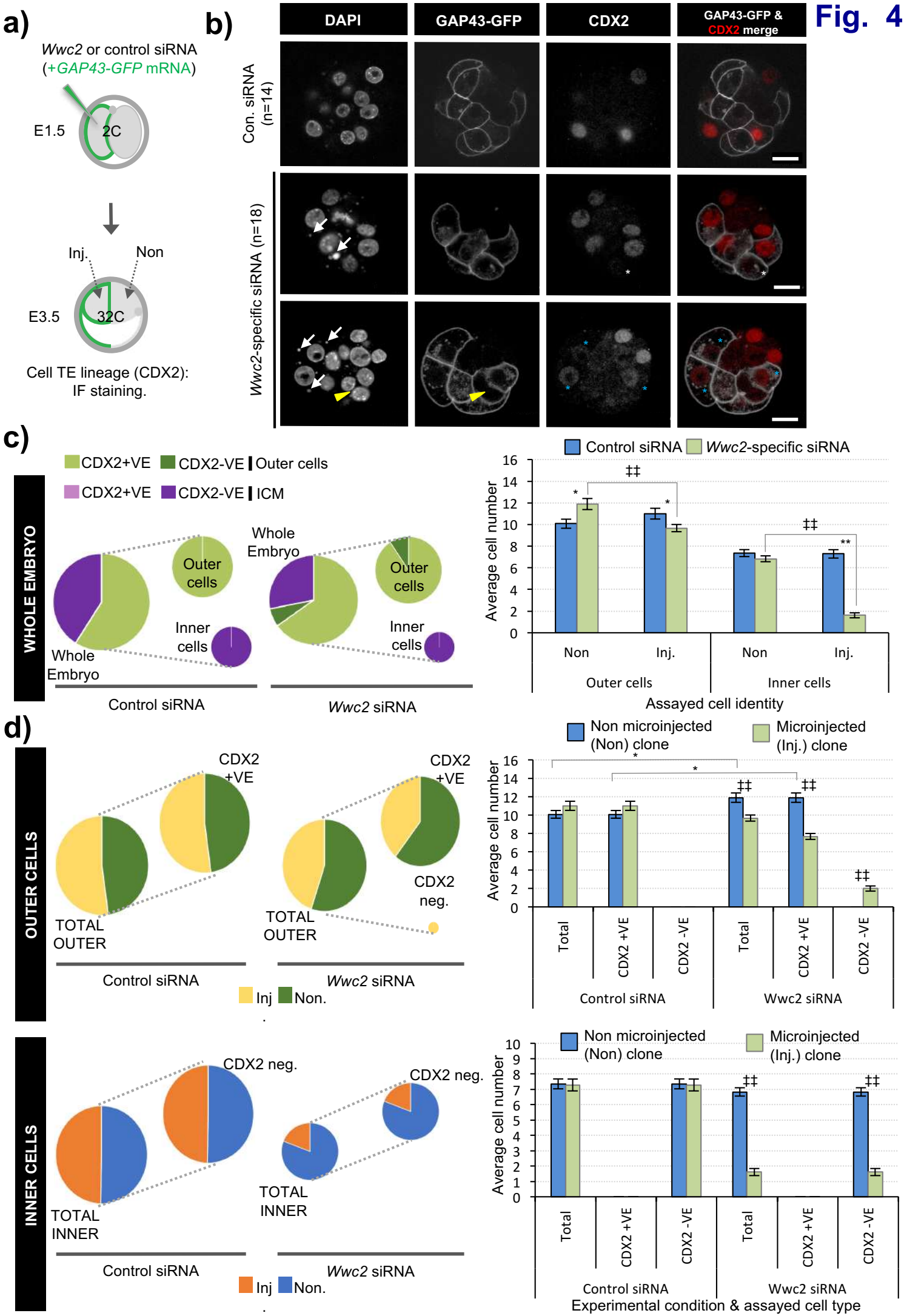
a)
Wwc2 or control siRNA
(+GAP43-GFP mRNA)
E1.5
2C
Inj.
Non
E3.5
32C
Cell TE lineage (CDX2):
IF staining.
b)
DAPI
GAP43-GFP
CDX2
GAP43-GFP & CDX2 merge
Con. siRNA (n=14)
Wwc2-specific siRNA (n=18)
c)
CDX2+VE
CDX2-VE
Outer cells
CDX2+VE
CDX2-VE
ICM
WHOLE EMBRYO
Whole Embryo
Outer cells
Inner cells
Control siRNA
Wwc2 siRNA
Control siRNA
Wwc2-specific siRNA
Average cell number
Non
Inj.
Outer cells
Inner cells
Assayed cell identity
d)
OUTER CELLS
CDX2 +VE
TOTAL OUTER
CDX2 neg.
Control siRNA
Wwc2 siRNA
Inj
Non.
Non microinjected (Non) clone
Microinjected (Inj.) clone
Total
CDX2 +VE
CDX2 -VE
Control siRNA
Wwc2 siRNA
INNER CELLS
CDX2 neg.
TOTAL INNER
Experimental condition & assayed cell type

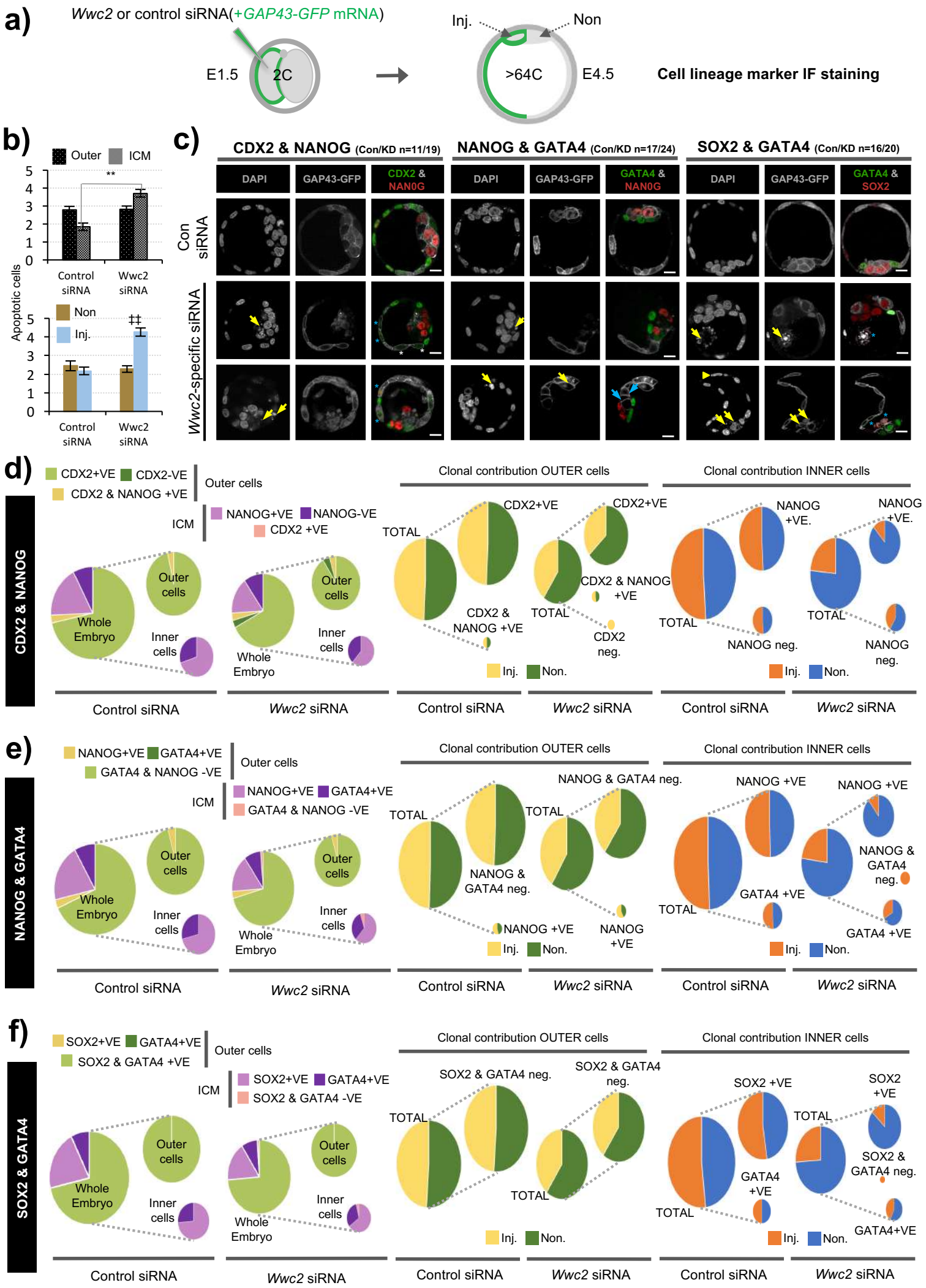
a)
Wwc2 or control siRNA(+GAP43-GFP mRNA)
E1.5
2C
Inj.
Non
>64C
E4.5
Cell lineage marker IF staining
b)
Outer
ICM
Apoptotic cells
Control siRNA
Wwc2 siRNA
Non
Inj.
c)
CDX2 & NANOG (Con/KD n=11/19)
NANOG & GATA4 (Con/KD n=17/24)
SOX2 & GATA4 (Con/KD n=16/20)
DAPI
GAP43-GFP
CDX2 & NANOG
GATA4 & NANOG
GATA4 & SOX2
Con siRNA
Wwc2-specific siRNA
d)
CDX2 & NANOG
CDX2+VE
CDX2-VE
CDX2 & NANOG +VE
Outer cells
ICM
NANOG+VE
NANOG-VE
CDX2 +VE
Clonal contribution OUTER cells
Clonal contribution INNER cells
Whole Embryo
Inner cells
TOTAL
CDX2 & NANOG +VE
CDX2 neg.
NANOG +VE.
NANOG neg.
Inj.
Non.
Control siRNA
Wwc2 siRNA
e)
NANOG & GATA4
NANOG+VE
GATA4+VE
GATA4 & NANOG -VE
NANOG & GATA4 neg.
GATA4 +VE
f)
SOX2 & GATA4
SOX2+VE
GATA4+VE
SOX2 & GATA4 +VE
SOX2 & GATA4 -VE
SOX2 & GATA4 neg.
SOX2 +VE
SOX2 +VE
GATA4 +VE
GATA4+VE

Fig. 5

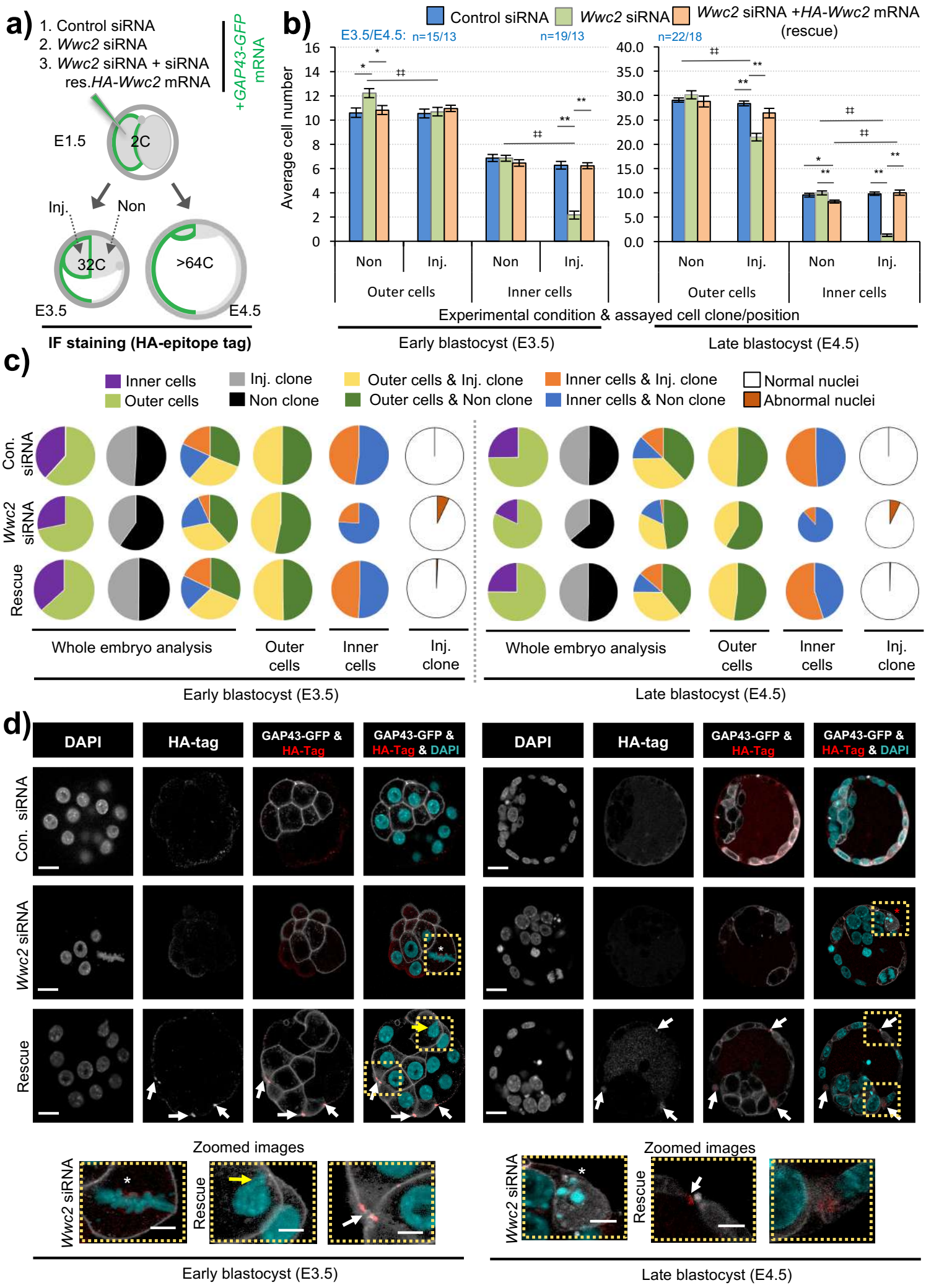
a)
1. Control siRNA
2. Wwc2 siRNA
3. Wwc2 siRNA + siRNA res.HA-Wwc2 mRNA
+GAP43-GFP mRNA
E1.5
2C
Inj.
Non
32C
>64C
E3.5
E4.5
IF staining (HA-epitope tag)
b)
Control siRNA
Wwc2 siRNA
Wwc2 siRNA +HA-Wwc2 mRNA (rescue)
E3.5/E4.5: n=15/13
n=19/13
n=22/18
Average cell number
Non
Inj.
Outer cells
Inner cells
Experimental condition & assayed cell clone/position
Early blastocyst (E3.5)
Late blastocyst (E4.5)
c)
Inner cells
Outer cells
Inj. clone
Non clone
Outer cells & Inj. clone
Outer cells & Non clone
Inner cells & Inj. clone
Inner cells & Non clone
Normal nuclei
Abnormal nuclei
Con. siRNA
Wwc2 siRNA
Rescue
Whole embryo analysis
Outer cells
Inner cells
Inj. clone
Early blastocyst (E3.5)
Late blastocyst (E4.5)
d)
DAPI
HA-tag
GAP43-GFP & HA-Tag
GAP43-GFP & HA-Tag & DAPI
Con. siRNA
Wwc2 siRNA
Rescue
Zoomed images
Wwc2 siRNA
Rescue
Early blastocyst (E3.5)
Late blastocyst (E4.5)

Fig. 6

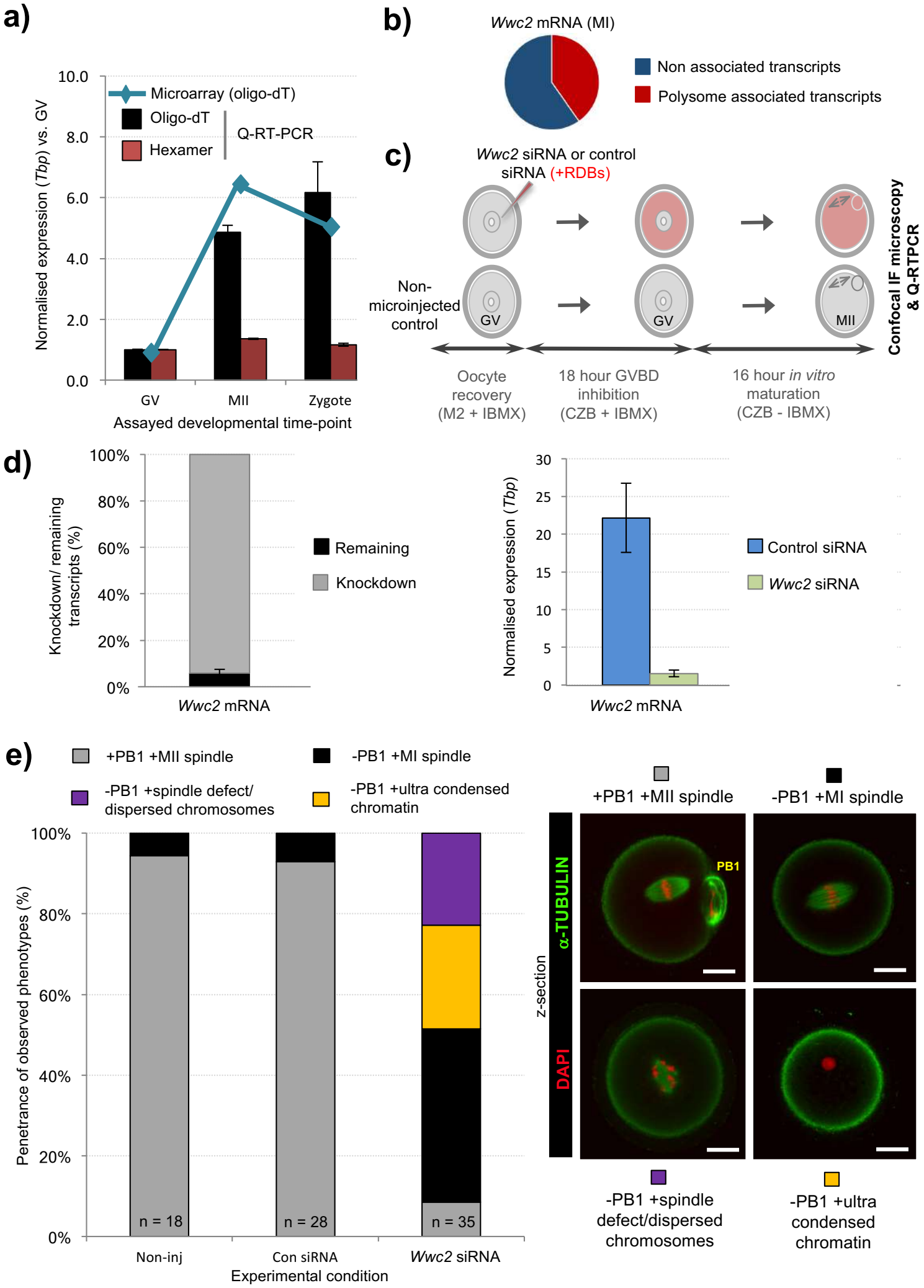
a)
Microarray (oligo-dT)
Oligo-dT
Hexamer
Q-RT-PCR
Normalised expression (Tbp) vs. GV
10.0
8.0
6.0
4.0
2.0
0.0
GV
MII
Zygote
Assayed developmental time-point
b)
Wwc2 mRNA (MI)
Non associated transcripts
Polysome associated transcripts
c)
Wwc2 siRNA or control siRNA (+RDBs)
Non-microinjected control
GV
GV
MII
Confocal IF microscopy & Q-RTPCR
Oocyte recovery (M2 + IBMX)
18 hour GVBD inhibition (CZB + IBMX)
16 hour in vitro maturation (CZB - IBMX)
d)
Knockdown/ remaining transcripts (%)
100%
80%
60%
40%
20%
0%
Remaining
Knockdown
Wwc2 mRNA
Normalised expression (Tbp)
30
25
20
15
10
5
0
Control siRNA
Wwc2 siRNA
Wwc2 mRNA
e)
+PB1 +MII spindle
-PB1 +MI spindle
-PB1 +spindle defect/ dispersed chromosomes
-PB1 +ultra condensed chromatin
Penetrance of observed phenotypes (%)
100%
80%
60%
40%
20%
0%
n = 18
n = 28
n = 35
Non-inj
Con siRNA
Wwc2 siRNA
Experimental condition
+PB1 +MII spindle
-PB1 +MI spindle
α-TUBULIN
DAPI
z-section
PB1
-PB1 +spindle defect/dispersed chromosomes
-PB1 +ultra condensed chromatin

Fig. 7

Fig. 8

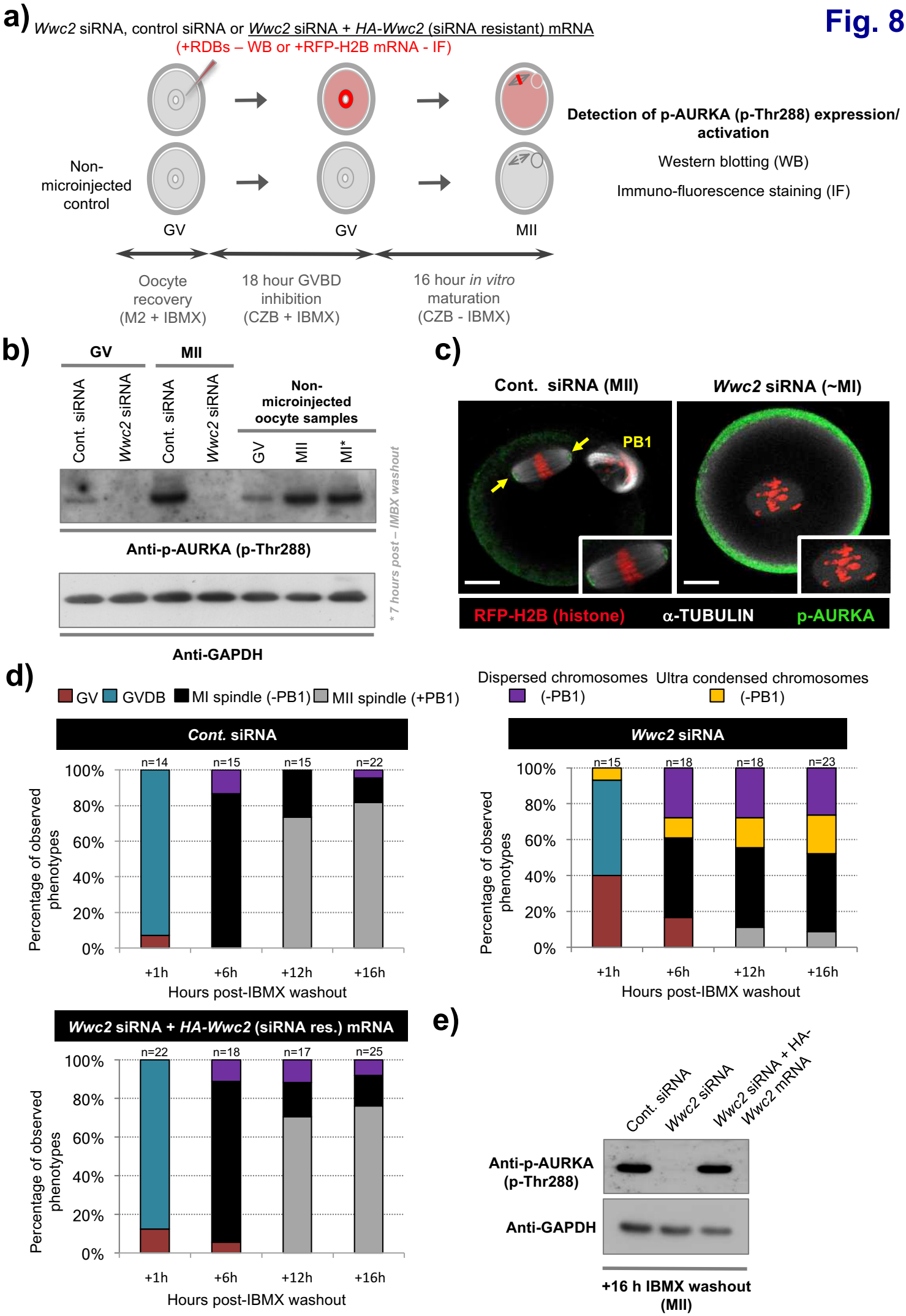
a)
Wwc2 siRNA, control siRNA or Wwc2 siRNA + HA-Wwc2 (siRNA resistant) mRNA
(+RDBs – WB or +RFP-H2B mRNA - IF)
Non-microinjected control
GV
GV
MII
Detection of p-AURKA (p-Thr288) expression/ activation
Western blotting (WB)
Immuno-fluorescence staining (IF)
Oocyte recovery (M2 + IBMX)
18 hour GVBD inhibition (CZB + IBMX)
16 hour in vitro maturation (CZB - IBMX)
b)
GV
MII
Cont. siRNA
Wwc2 siRNA
Cont. siRNA
Wwc2 siRNA
Non-microinjected oocyte samples
GV
MII
MI*
Anti-p-AURKA (p-Thr288)
Anti-GAPDH
* 7 hours post – IMBX washout
c)
Cont. siRNA (MII)
Wwc2 siRNA (~MI)
PB1
RFP-H2B (histone)
α-TUBULIN
p-AURKA
d)
GV
GVDB
MI spindle (-PB1)
MII spindle (+PB1)
Dispersed chromosomes (-PB1)
Ultra condensed chromosomes (-PB1)
Cont. siRNA
Wwc2 siRNA
Wwc2 siRNA + HA-Wwc2 (siRNA res.) mRNA
Percentage of observed phenotypes
100%
80%
60%
40%
20%
0%
n=14
n=15
n=15
n=22
n=15
n=18
n=18
n=23
n=22
n=18
n=17
n=25
+1h
+6h
+12h
+16h
Hours post-IBMX washout
e)
Cont. siRNA
Wwc2 siRNA
Wwc2 siRNA + HA-Wwc2 mRNA
Anti-p-AURKA (p-Thr288)
Anti-GAPDH
+16 h IBMX washout (MII)